THESIS

STRATIGRAPHIC FEEDBACKS ON ALTERNATE BAR MORPHOLOGY

Submitted by

Ryan A. Brown

Department of Civil and Environmental Engineering

In partial fulfillment of the requirements

For the Degree of Master of Science

Colorado State University

Fort Collins, Colorado

Summer 2017

Master's Committee:

Advisor: Peter A. Nelson

Ryan R. Morrison
Sara L. Rathburn

ABSTRACT

STRATIGRAPHIC FEEDBACKS ON ALTERNATE BAR MORPHOLOGY

As gravel bed rivers aggrade, they can develop subsurface stratigraphy consisting of heterogeneous grain-size distributions in the downstream, cross-stream, and vertical directions. During subsequent periods of degradation, this heterogeneous stratigraphy can be exhumed and may feedback on the processes that drive morphodynamic evolution. However, these surface-stratigraphy feedbacks are poorly understood and difficult to predict. These feedbacks are investigated by implementing the ability to store, track, and access bed stratigraphy in the 2-dimensional mixed-grain-size morphodynamic model FaSTMECH. The stratigraphy framework consists of a 3-dimensional grid of subsurface layers containing grain size fractions. The active layer (surface) is then allowed to exchange sediment with bedload as well as the stratigraphy layers. During aggradation, size fractions of sediment in the active layer and bedload are mixed with the highest stratigraphy layer size fractions. During degradation, the active layer takes on the sediment properties stored in the stratigraphy. This model is used to investigate stratigraphic feedbacks on the coevolution of surface patchiness and alternate bar morphology. When alternate bars are forced by an obstruction, differences between model simulations with and without stratigraphy enabled are minimal because bars quickly stabilize and become fixed. With no obstruction, however, migrating alternate bars formed with stratigraphy enabled are wider and display stronger sorting patterns than those formed without accounting for stratigraphy. The repeated aggradation and degradation associated with bar migration results in frequent interaction between subsurface and surface material. The repeated access of material finer than the initial bulk material during degradation allows for greater degrees of surface sorting where coarse bar tops become coarser and fine pools become finer. Changes in sorting patterns are shown to increase bar width and increase bar celerity by 1 cm/min. This suggests that surface/subsurface interactions play an important role in setting bed morphology, sorting patterns, and bedform dynamics in gravel bed rivers.

ACKNOWLEDGMENTS

This work was supported by the American Chemical Society Petroleum Research Fund (Grant 53837-DNI8) and the National Science Foundation (Grant EAR-1455259). Thank you to my advisor Dr. Peter Nelson for the opportunity to work on this project, the guidance and motivation to keep working, and for sitting at the computer staring at Fortran code with me when things just weren't working right. Thank you to my committee remembers, Dr. Ryan Morrison and Dr. Sara Rathburn, for invaluable feedback on this work. Thanks to my friends in the office, Dan Brogan, Jacob Morgan, Andy Bankert, Tess Hanson, and Mike Gieschen, for good times, encouragement, and lots of MATLAB help. A huge hug and many thanks to my parents, grandparents, and brother for all the love and for supporting me down my circuitous, long path to this degree. Lastly, this wouldn't have been possible without the much needed encouragement, weekend adventures, love, and editing from Annette Patton, Copper, and Juniper.

TABLE OF CONTENTS

1 Introduction

It has been widely shown that gravel-bedded rivers and laboratory flumes can develop patches with distinct grain size and sorting [*Dietrich et al.*, 1989; *Lisle et al.*, 1991; *Lisle and Madej*, 1992; *Lisle et al.*, 1993; *Crowder and Diplas*, 1997; *Buffington and Montgomery*, 1999; *Garcia et al.*, 1999; *Laronne et al.*, 2000; *Dietrich et al.*, 2005; *Nelson et al.*, 2009, 2010; *Yager et al.*, 2012; *Scheingross et al.*, 2013; *Ferrer-Boix and Hassan*, 2014; *Nelson et al.*, 2014; *Legleiter*, 2014]. These patches have also been shown to develop into fairly predictable patterns based on channel planform. In particular, this sorting develops into coarse bar tops and fine pools in straight channels [e.g. *Mosley and Tindale*, 1985; *Lisle and Madej*, 1992; *Nelson et al.*, 2010], while curved or meandering channels display the opposite sorting of fine bar tops and coarse pools [e.g. *Bluck*, 1971; *Bridge and Jarvis*, 1976; *Whiting and Dietrich*, 1991; *Clayton*, 2010].

Bed surface patches create spatially variable hydraulic roughness, which in turn produces spatial variations in velocity, depth, boundary shear stress, and sediment flux. These roughness feedbacks can have a significant influence on the evolution of bed topography and surface sorting [*Nelson et al.*, 2015b]. The *Nelson et al.* [2010] laboratory flume observations of sediment sorting and transport in a straight channel with alternate bars showed that the formation of coarse bar tops and fine pools is due to grain-size-selective cross-stream sediment transport, where declining shear stress over the bar top causes fine sediment to be laterally transported into adjacent pools. Building upon that work, *Nelson et al.* [2015a] developed a mixed-grain-size two-dimensional morphodynamic model to allow direct calculation of the coevolution of bed topography and bed-surface patches, confirming the mechanism of size-selective cross-stream sediment flux accommodating topographically forced boundary shear stress divergence. Although the model predicted overall sorting patterns well, the relative degree of sorting was underpredicted; *Nelson et al.* [2015a] suggested that this underprediction may have been a consequence of the lack of a stratigraphy storage submodel.

Self-formed stratigraphy may interact with and feed back on the bed surface or active layer [*Hirano*, 1971; *Parker*, 2008] when a river displays strong sorting patterns in migrating bedforms, as can be the case for migrating alternate bars. In a straight channel, as a coarse bar migrates into and through a pool, the fine surface sediment in the pool becomes buried. As bar migration continues, the buried fine sediment may be reexposed, and its roughness effects on the flow field will then affect channel evolution in potentially complex ways.

In this study, I use the two-dimensional (2D) morphodynamic model FaSTMECH to explore feedbacks between self-formed stratigraphy and alternate bar dynamics in gravel-bedded channels. Morphodynamic models compute the flow field, which is then used to compute the sediment transport field, which is then used to update the bed elevation and surface grain-size distribution (Figure 1). The model is considered to be semi-coupled where the hydraulics and sediment transport rates are calculated, and then the bed evolution and surface grain-size distribution are calculated separately. As such, an important assumption with this model is that the bed morphology and surface grain sizes do not change dramatically within a given time step.

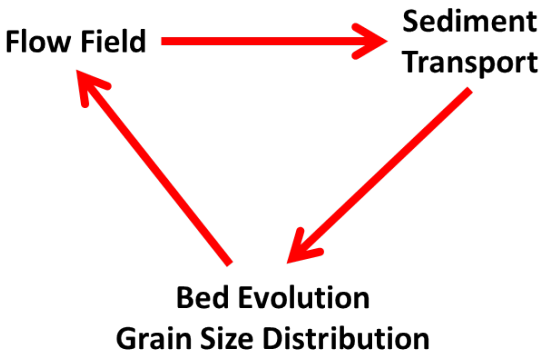

Figure 1: Morphodyanmic triangle flow chart showing progression of solution scheme for each time step.

The ability to develop, store, and access stratigraphy has been implemented in some one-dimensional and, to a lesser extent, two-dimensional morphodynamic models. As part of an investigation into downstream fining, *Hoey and Ferguson* [1994] used a one-dimensional (1D), mixed-grain-size model in which the subsurface is discretized into five layers of sediment, whose thickness changed depending on whether the channel was experiencing aggradation or degradation. The DREAM model developed by *Cui et al.* [2006] also includes some reference to storage of grain sizes in the subsurface, though it is unclear from the published

study exactly how it is accomplished. The stratigraphy component of both of these 1D models was not validated against field or flume data.

The first study to clearly describe *and* validate a stratigraphy framework for implementation into a mixed-grain-size morphodynamic model is presented by *Viparelli et al.* [2010]. In their framework, a stack of equal thickness layers exists below the active surface layer. This stack stores grain size information and can be modified and accessed accordingly during periods of aggradation or degradation. Most important is that when validated against flume experiments, it was found that the framework adequately describes the development, storage, and access of stratigraphy. This model was then utilized to model the evolution of the gravel bedded Trinity River in Northern California under a cyclic hydrograph anthropomorphically imposed through dam releases [*Viparelli et al.*, 2011].

In an effort to move away from the active layer concept, *Parker et al.* [2000] and *Peng et al.* [2014] presented alternative formulations for the development, storage, and access of stratigraphy. The probabilistic Exner sediment continuity relation derived by *Parker et al.* [2000] has the potential to provide a useful future route for studies involving vertical sorting, but to date such a model has not been successfully implemented. The *Peng et al.* [2014] study presents what they call a surface-based formulation for sediment continuity. This method essentially modifies the sediment exchange fraction (discussed later and in the Appendix) and provides a stronger physical basis for determining the grain size fractions at the interface of the surface and subsurface layers. It was found that when using the surface-based formulation, the morphodynamic model performed as well or better than when using the traditional active layer formulation.

Vertical sorting has also been investigated in laboratory experiments. Experiments focused on downstream fining presented by *Seal et al.* [1997] note that the surface grain size is always coarser than the deposits in the bed directly below a given location. While vertical sorting is noted, its importance in the development of downstream fining is not clearly discussed. In another study on downstream fining, *Toro-Escobar et al.* [2000] present limited

vertical sorting data from a flume experiment and they note that the subsurface generally fines downstream to a smaller degree than the surface. Flume experiments by *Bankert* [2016] show that vertical sorting has potentially strong feedbacks on alternate bar dynamics under varying sediment supplies. In particular, it was found that lateral erosion of alternate bars during degradation was halted due to coarse layers stored within the bars. Overall, these experiments show that vertical sorting can have a substantial control on bed morphology during periods of widespread degradation.

In this paper, I modify the mixed-grain-size morphodynamic model FaSTMECH [*Nelson et al.*, 2015a] to include a stratigraphy framework based on the 1D model presented by *Viparelli et al.* [2010]. In this framework, the ability to compute, store, and access stratigraphy involves modifying the bed evolution/grain-size distribution leg of the triangle in Figure 1. Therefore, if stored stratigraphy modifies the surface grain-size distribution, it has the potential to feedback on the flow solution through grain roughness feedbacks. I use this model to seek answers to the following questions: What is the stratigraphic signature of bar migration? And how does stratigraphy influence sediment sorting, bar morphology, and bar dynamics? I hypothesize that incorporating stratigraphic feedbacks in model simulations will result in a greater degree of sorting between bars and pools when compared to model simulations without stratigraphic feedbacks, especially for conditions where bars are freely migrating downstream.

2 Methods

2.1 FaSTMECH Mixed-Grain-Size Model

The one-dimensional stratigraphy model developed by *Viparelli et al.* [2010] was modified for two-dimensional applications and implemented in FaSTMECH, a two-dimensional, quasi-steady, morphodynamic model. FaSTMECH was originally developed by *Nelson and McDonald* [1995] and is now included as a solver in the free International River Interface Cooperative (www.i-ric.org) software package. This model has recently been modified by *Nelson et al.* [2015a] to incorporate mixed-grain-size sediment transport and sediment continuity calculations.

Details of the equations, assumptions, and parameters used by the FaSTMECH model are described in the Appendix and only a brief description is provided here. FaSTMECH solves the vertically averaged steady-state equations of fluid mass and momentum in a curvilinear orthogonal coordinate system. Shear stresses are computed using a drag coefficient closure incorporating a roughness coefficient, C_d, which is defined using the law of the wall:

$$C_d = \left[\frac{1}{\kappa}\left(\ln\frac{h}{z_0} - 1\right)\right]^{-2} \tag{1}$$

where κ is von Karman's constant ($\kappa \approx 0.41$), h is the local flow depth, and z_0 is the roughness height corresponding to the height above the bed where the velocity is approximately zero. The roughness height z_0 is parameterized to be proportional to the 84th percentile surface grain size (D_{84}) [*Dietrich and Whiting*, 1989]:

$$z_0 = 0.1 D_{84}. \tag{2}$$

This linkage between surface grain size and hydraulic roughness allows the model to simulate complex feedbacks between bed topography and surface patchiness.

As the analysis performed by *Nelson et al.* [2015a] studied sorting in gravel-bedded rivers, the *Parker* [1990] bedload relation for mixed-grain-size transport was chosen. An overview of this relation is provided in the Appendix. An important limitation of this relation is that the input grain-size distribution is truncated at 2 mm (grain sizes smaller than 2 mm are eliminated from the distribution). This is not an issue for the simulations presented in this study, as they use fully gravel-sized distributions (all grains are equal to or larger than 2 mm). However, if used for scenarios where the bed has a high sand fraction, the mixed-grain-size capabilities would yield unsatisfactory results. Efforts are currently underway to implement the *Wilcock and Crowe* [2003] bedload relation, which would allow for simulations using sediment mixtures with nontrivial sand fractions.

Mixed-grain-size bed evolution is accomplished using the active layer method first developed by *Hirano* [1971] and modified for mixed-grain-size sediment by *Parker* [1992, 2008]. The bed evolution over a time step and the surface grain-size distribution (F_i) are computed using first-order explicit Euler schemes to the following equations respectively:

$$(1-\lambda_p)\frac{\partial \eta}{\partial t} = -\vec{\nabla}\cdot\vec{q}_{bT} \tag{3}$$

and

$$(1-\lambda_p)\left[L_a\frac{\partial F_i}{\partial t} + (F_i - f_{li})\frac{\partial L_a}{\partial t}\right] = -\vec{\nabla}\cdot\vec{q}_{bi} + f_{li}\vec{\nabla}\cdot\vec{q}_{bT}. \tag{4}$$

where λ_p is the bed porosity (assumed to be 0.35), η is the bed elevation (m), t is time (s), $\vec{q}_{bT}$ is the unit volumetric total bedload rate ($^{m^2}/_{s}$), $\vec{q}_{bi}$ is the unit volumetric bedload rate of size class i ($^{m^2}/_{s}$), L_a is the active layer thickness ($L_a = 2 \cdot D_{90}$), and f_{li} is the exchange fraction. The exchange fraction is defined as the fraction of the i^{th} size class at the boundary of the active layer (surface) and the subsurface. The exchange fraction accounts for either transfer of material from the subsurface during degradation, or for the mixing of bedload and surface material in the active layer during aggradation. It is computed using Equations 19 and 20 in the Appendix.

2.2 Stratigraphy Framework

While Equation 4 allows for spatial and temporal variability in the surface grain-size distribution, it does not store or access vertical variability in the grain-size distribution of the subsurface. During periods of aggradation, the exchange fraction, f_{li}, is assumed to be a mixture of the active layer and bedload grain-size distributions [*Hoey and Ferguson*, 1994; *Toro-Escobar et al.*, 1996]. During periods of degradation, f_{li} is simply the distribution of the assumed homogeneous bulk subsurface. Because the subsurface distribution is not a function of the surface and bedload distributions, the surface grain-size distribution calculated by Equation 4 is not modified by vertical heterogeneity of grain-size distributions. This lack of stratigraphy storage is noted as a potentially important limitation of the mixed-grain-size model implemented by *Nelson et al.* [2015a].

To remedy this limitation, a modified version of the 1D stratigraphy framework presented by *Viparelli et al.* [2010] was added to the mixed-grain-size bed evolution routine. Minimal modification was needed to convert the framework from 1D to 2D. A brief summary of the 2D framework follows and a more detailed description is presented in the Appendix.

The stratigraphy framework comes in two parts, one corresponding to periods of aggradation, the other for periods of degradation. To store and access the stratigraphy during these two cases, a discretization of the subsurface is performed by dividing the vertical space below each grid point into a series of layers with a predefined thickness (L_s). For this study this thickness is held constant at 2 cm. This thickness provides adequate vertical resolution of the stratigraphy without becoming too memory intensive. The Appendix has a detailed description of how this grid is defined and how it is modified during aggradation and degradation.

The more complex condition of aggradation involves storing the grain size fractions of some mixture of the subsurface, surface, and bedload. The mixture of these materials is a vertical distance (thickness) weighted average of the exchange fraction and existing subsurface fractions already stored in the node. The existing subsurface material is given a weight

corresponding to the initial thickness of the stratigraphy layer. The exchange fraction is given a weight corresponding to the added thickness after aggradation. The formation of this varied stratigraphy in the alternate bars is shown schematically in Figure 2.

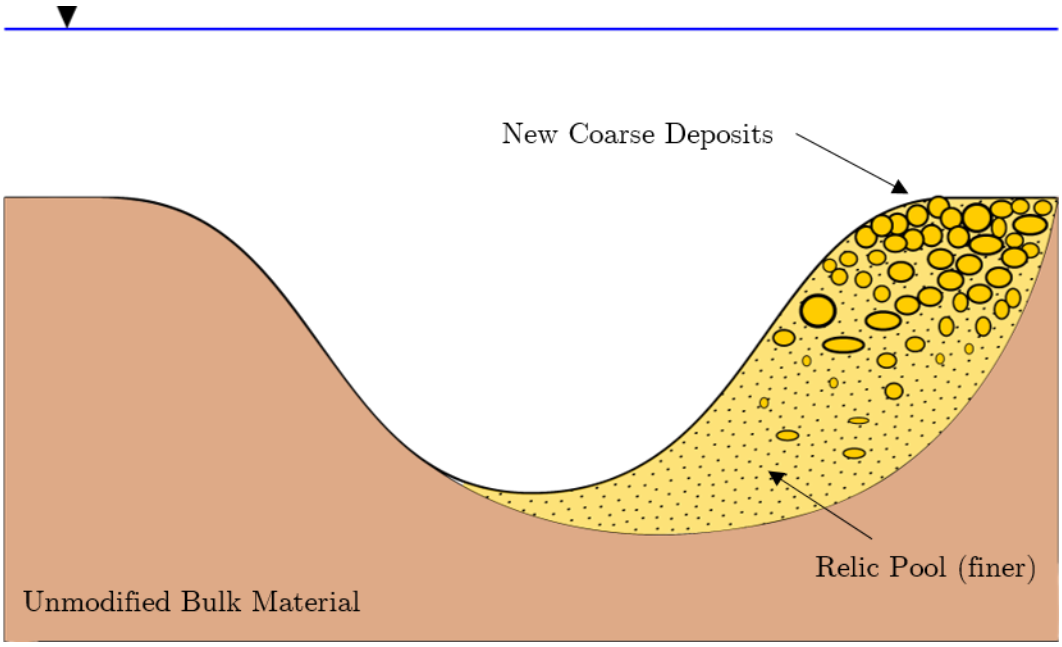

Figure 2: Schematic showing formation of vertical sorting through an alternate bar during a phase of aggradation.

Degradation is considerably more simple to implement. If the elevation of a grid point decreases, the exchange fraction simply takes on the distribution stored in the stratigraphy layer corresponding to the elevation of the subsurface/active layer interface. This now allows for the surface distribution to be partially dependent upon any stored vertical grain sorting.

The stratigraphy framework has only one direct user input parameter, the stratigraphy layer thickness, L_s. This parameter has no direct effect on any of the numerical schemes utilized to solve the various governing equations. Therefore, the model is not numerically sensitive to changes in this parameter. Most simply, it is viewed as the resolution at which one wishes to view the subsurface. Furthermore, the division of the subsurface into a discrete number of constant thickness layers has minimal physical meaning, as the subsurface in a real system will be comprised of layers of varying thickness. While not directly investigated, it is possible for the value of L_s to modify to the results of the model. The grain size distribution

associated with each layer can be thought of as an average of varied distributions contained within that layer. If L_s is decreased the resolution of the stratigraphy is decreased and not as much detail is stored in the subsurface. Furthermore, the increased thickness suggests that more averaging of grain size heterogeneity occurs within a single layer. Therefore, one would expect the stratigraphic signatures to be muted and result in a less dramatic stratigraphic feedback on the flow and sediment transport fields. The converse may also be said if L_s is decreased. This increases the stratigraphic resolution which could allow for a stronger stratigraphic signature and stronger stratigraphic feedbacks.

2.3 Simulation Scenarios

Two straight channel flume scenarios were chosen to investigate the effects of stratigraphy. Scenario 1 simulates a St. Anthony Falls Laboratory (SAFL) near-field scale flume experiment described by *Nelson et al.* [2010] and used by *Nelson et al.* [2015a,b] for numerical simulations. In the experiment, an obstruction was placed at the upstream end of the flume, blocking one-third of the flume width. This obstruction forced the formation of alternate bars. Scenario 2 simulates a 200-meter-long straight flume channel of the same width as Scenario 1, however no obstruction is placed at the upstream end of the flume. Without this obstruction, free forming, migrating alternate bars develop.

Each scenario was run with and without stratigraphy. With all other parameters and variables held constant between simulations, the stratigraphy framework was enabled in one run and disabled in another. Differences between the simulations with and without stratigraphy enabled can then be directly attributed to the effects of vertical sorting.

2.3.1 Scenario 1 - Forced Alternate Bars

Scenario 1 is a simulation of an experiment performed at SAFL in the main flume. The flume is a straight, concrete channel that measures 2.75 m wide by 1.8 m deep by 83.8 m long (Figure 3). For this experiment a constant water discharge of 0.4 ± 0.02 cms was supplied.

Only the lower 55 m of the channel was simulated in this study, however, because the data acquisition cart could not collect data for the upstream portion (Figure 3). The initial bed slope was 0.0137. A gravel mixture between 2 mm and 45 mm (Figure 4) was used for the initial bulk material in the flume. For the upstream sediment supply conditions, sediment was recirculated.

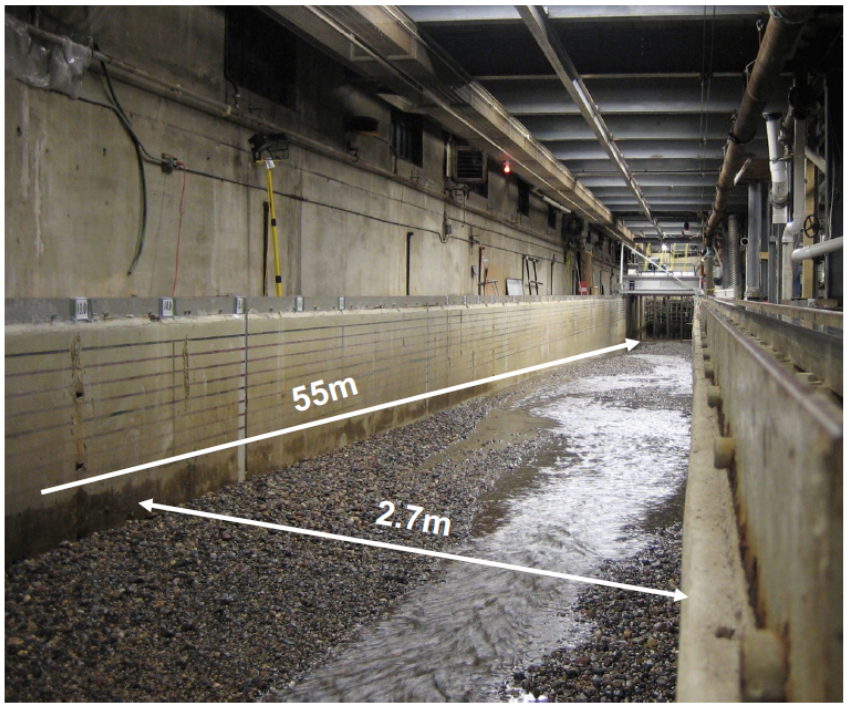

Figure 3: Alternate bar conditions observed during SAFL experiments with dimensions of simulated region noted.

Sediment leaving the flume was pumped back to the upstream end of the flume and fed into the flow. An obstruction (sand bags) was then placed at the upstream end of the 55 m long study length to constrict flow and sediment transport to the left two thirds of the channel. This was done to promote development of alternate bars as seen in Figure 3.

The simulation conditions for Scenario 1 are the same as those used in *Nelson et al.* [2015a] and closely match the experimental conditions in the SAFL flume. A 55 m long by 2.75 m wide grid with a square cell size of 12.5 cm is used with a plane bed initial condition set to a slope of 0.0137. As the initial bed in the SAFL experiment was

the well mixed distribution seen in Figure 4, both the initial surface and bulk subsurface distributions in the model were set to the experiment's bulk distribution. Additionally, to ensure the flow field is fully developed, a morphological boundary is imposed approximately 3 m downstream. Upstream of this boundary the bed elevation and surface grain-size distributions are not allowed to change for the entire simulation. Equilibrium conditions were achieved in 4.75 hours of simulation time. A computational time step of 2 seconds was used which ensures that bed elevation and grain-size distribution changes are small; a condition necessary due to the semi-coupled nature of the model. This time step length is carried over from the simulations in *Nelson et al.* [2015a,b] and provides a reasonable compromise between bed evolution stability and computational time.

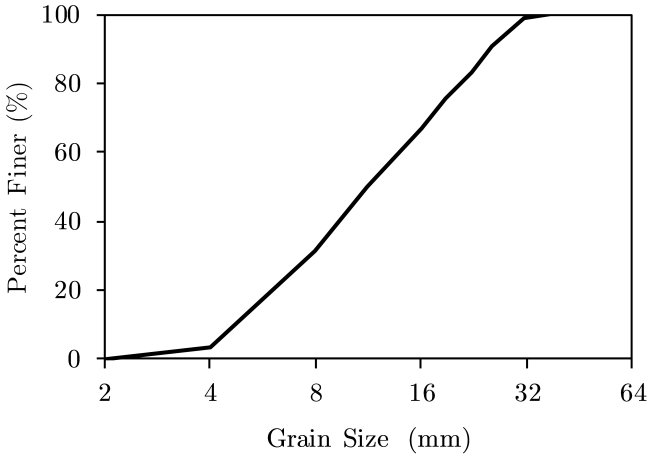

Figure 4: Grain size distribution of the bulk material used in both Scenario 1 and 2.

2.3.2 Scenario 2 - Free Alternate Bars

Scenario 2 simulates a 200 meter straight channel of the same width and slope as the SAFL simulation, however the upstream obstruction is removed to allow the formation of free alternate bars. Additionally, the upstream sediment condition is set equal to the transport capacity of the system to prevent any reach scale aggradation or degradation. The grain-size distribution is also forced to be constant across the upstream morphological boundary. This results in a simulation of a sediment feed flume where sediment is fed at a rate equal to what is being transported through the channel. As the spatial domain is increased, the time to reach a dynamic equilibrium state was also longer. Simulations were carried out using

the same 2-second time step with the overall duration increased to about 22 hrs. All other conditions and parameters are unchanged from Scenario 1.

3 Results

The results of each scenario are presented below. The primary analysis performed is a comparison of each scenario's results with and without stratigraphy enabled. When analyzing the bed elevations to determine differences, the detrended topography is used. This is the bed elevation with the bed slope removed, as though the bed was tilted such that the upstream and downstream bed elevations are the same. This ultimately makes bars and pools more visually distinct.

3.1 Scenario 1 - Stratigraphy Effects on Forced Alternate Bars

Due to the forcing of the upstream obstruction, two alternate bars form in Scenario 1. The development and persistence of these bars is shown in the plots of detrended topography in Figure 5 for a simulation run with stratigraphy enabled. The general shape, location, and wavelength of these features is similar to the results observed in the SAFL flume experiments. From the initial plane bed conditions, a bar quickly forms beginning around 1,500 seconds on the left side of the channel downstream of the obstruction. The location of this most upstream bar remains fairly constant for the entire simulation. Further downstream, a train of small amplitude migrating alternate bars form and gradually increase in size until one becomes somewhat stationary on the right side of the channel and begins to grow to a similar size as the upstream bar. This shows that there is a short period of cyclical degradation and aggradation for part of the simulation spatial and temporal domain.

The end dynamic equilibrium state for Scenario 1 is shown in Figure 6. From the detrended elevation plot the two bars develop to about the same size and shape. Additionally, the expected sorting pattern of coarse bar tops and fine pools is clearly visible.

The bed morphology (Figure 7) shows minimal difference between the simulations with and without stratigraphy enabled. The bars are in essentially the same location and their shapes are similar. Some minor differences can be seen in regards to the height of the bars

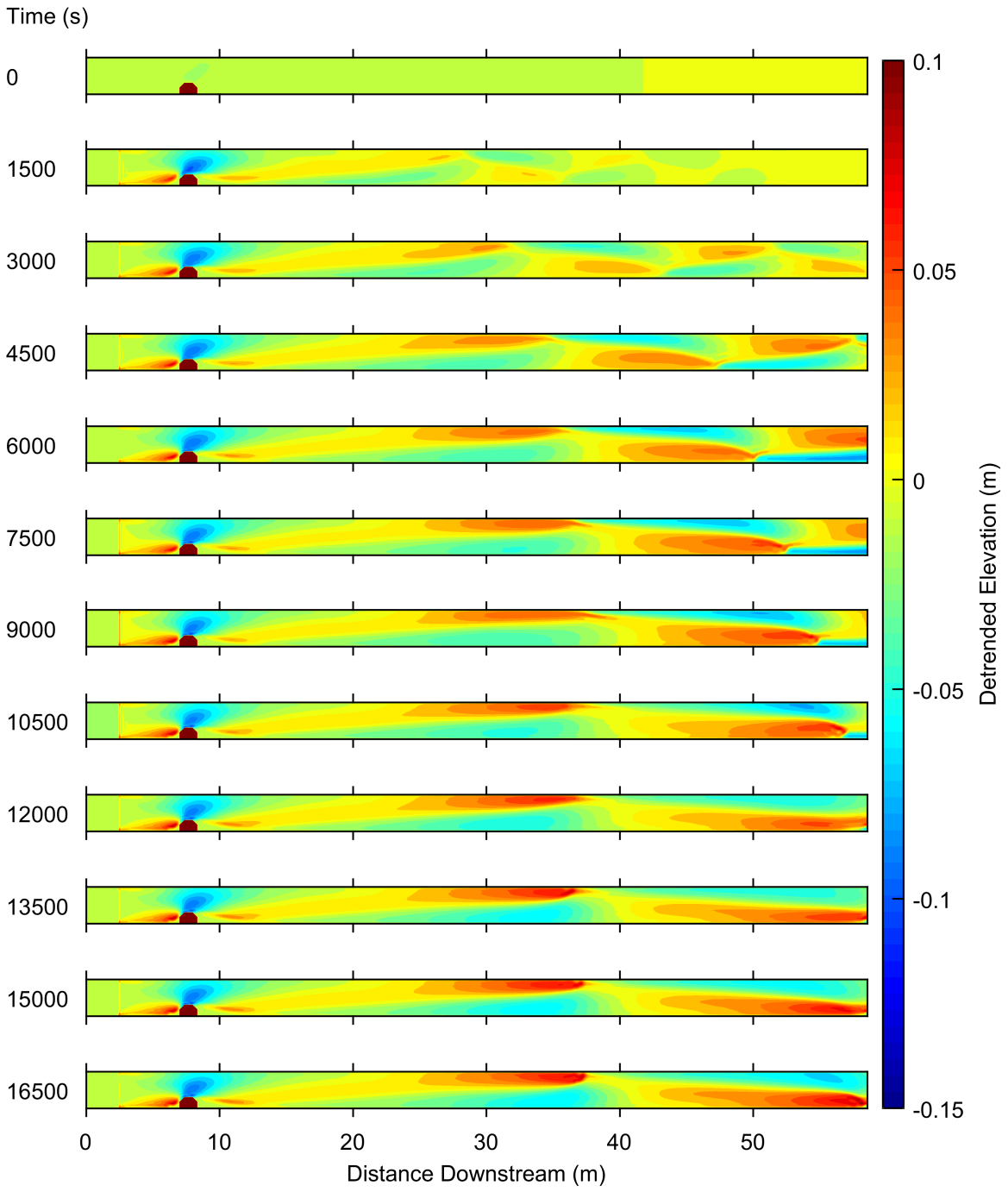

Figure 5: Detrended topography time series for Scenario 1 with stratigraphy enabled. The upstream obstruction is clearly seen as the high point roughly 8 meters downstream on channel right.

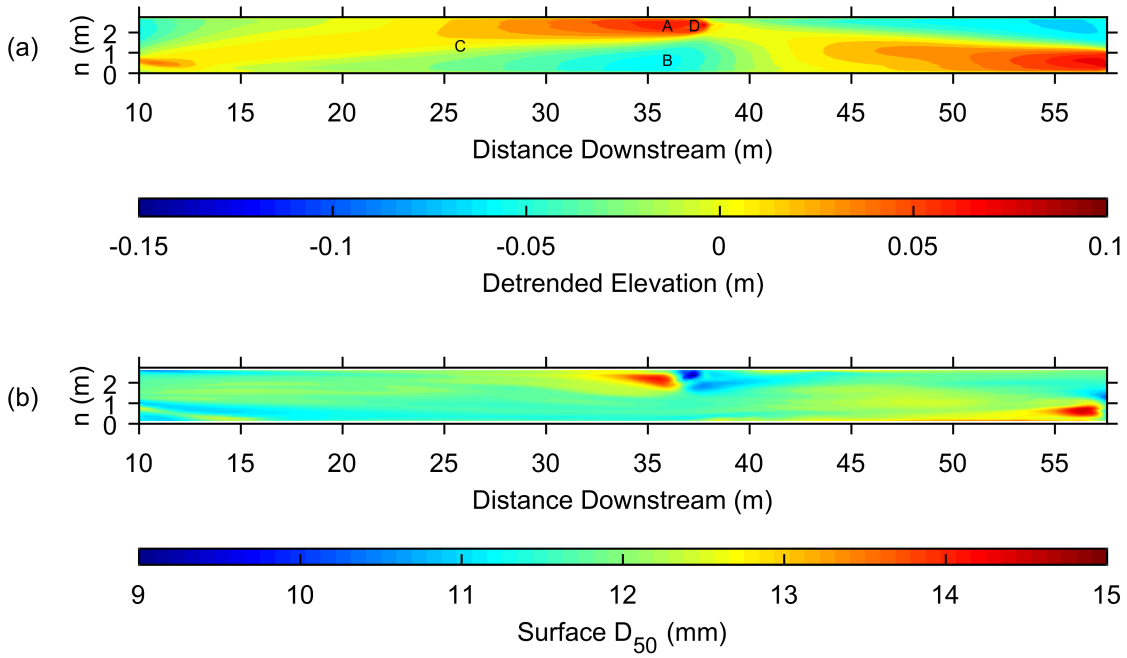

Figure 6: (a) Detrended topography and (b) surface median grain size at end (time = 17,000 s) of Scenario 1 simulation with stratigraphy enabled. Letters in (a) refer to locations of stratigraphy profiles shown in Figure 9.

and depth of the pools. Without stratigraphy enabled, the overall height of the upstream bar is about the same as the simulation with stratigraphy; however, there is a slightly larger area with this higher elevation. This is not observed at the downstream bar however. Looking at the pools, it is evident that the downstream pool has about the same depth between simulations. The deepest area is slightly increased when stratigraphy is enabled. Overall, there is no visibly significant change in bed morphology for Scenario 1 when stratigraphy is enabled.

While minimal changes are observed in terms of bed morphology, there are more noticeable changes to the median grain size in certain areas of the bed. Figure 8 shows the median (D_{50}) surface grain size for a simulation run with stratigraphy and one without stratigraphy enabled. Additionally, a difference map of the two D_{50} grids is shown in Figure 8c which depicts the quantitative change in the median grain size for each grid cell. The overall sorting

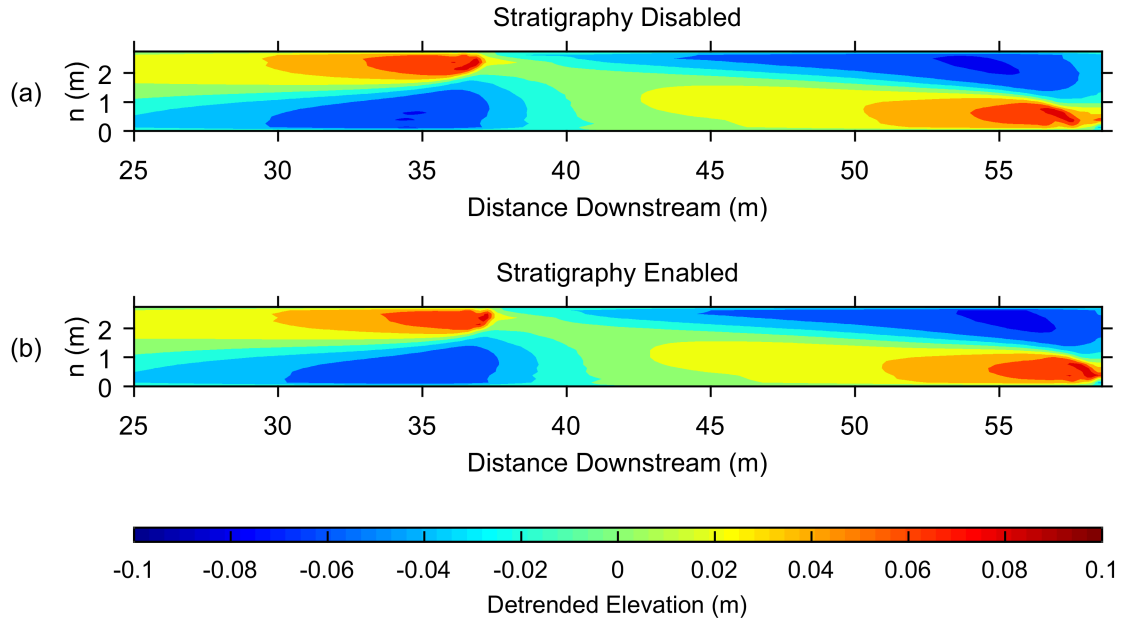

Figure 7: Comparison of the detrended topography between simulations (a) with and (b) without stratigraphy enabled for Scenario 1.

pattern is not altered between simulations. As expected, the bars tops are coarse and the pools are fine. What has changed is the degree of sorting; the difference between the median grain size in the pools and the bar tops is greater when stratigraphy is enabled. This is most easily seen on the left side of the channel at about 37 m. Here, the bar top has approximately the same median grain size for both simulations; however, the pool is considerably finer when stratigraphy tracking is enabled. These observations hold true as well for the downstream pool and bar (57 m). It is important to note that the areas identified as 1 to 2 mm coarser in the difference plot are most likely due to slight differences in where the bars are located between the two simulations. Through the entire domain, it is possible to see a very slight fining of the entire bed, with enhanced fining of the pools.

Velocity magnitude and streamline patterns for Scenario 1 are roughly identical between simulations run with and without stratigraphy enabled. As expected, the highest velocities are through each pool and adjacent to the obstruction. The same can also be said for shear stress and overall bedload transport rates. Both are essentially unchanged between

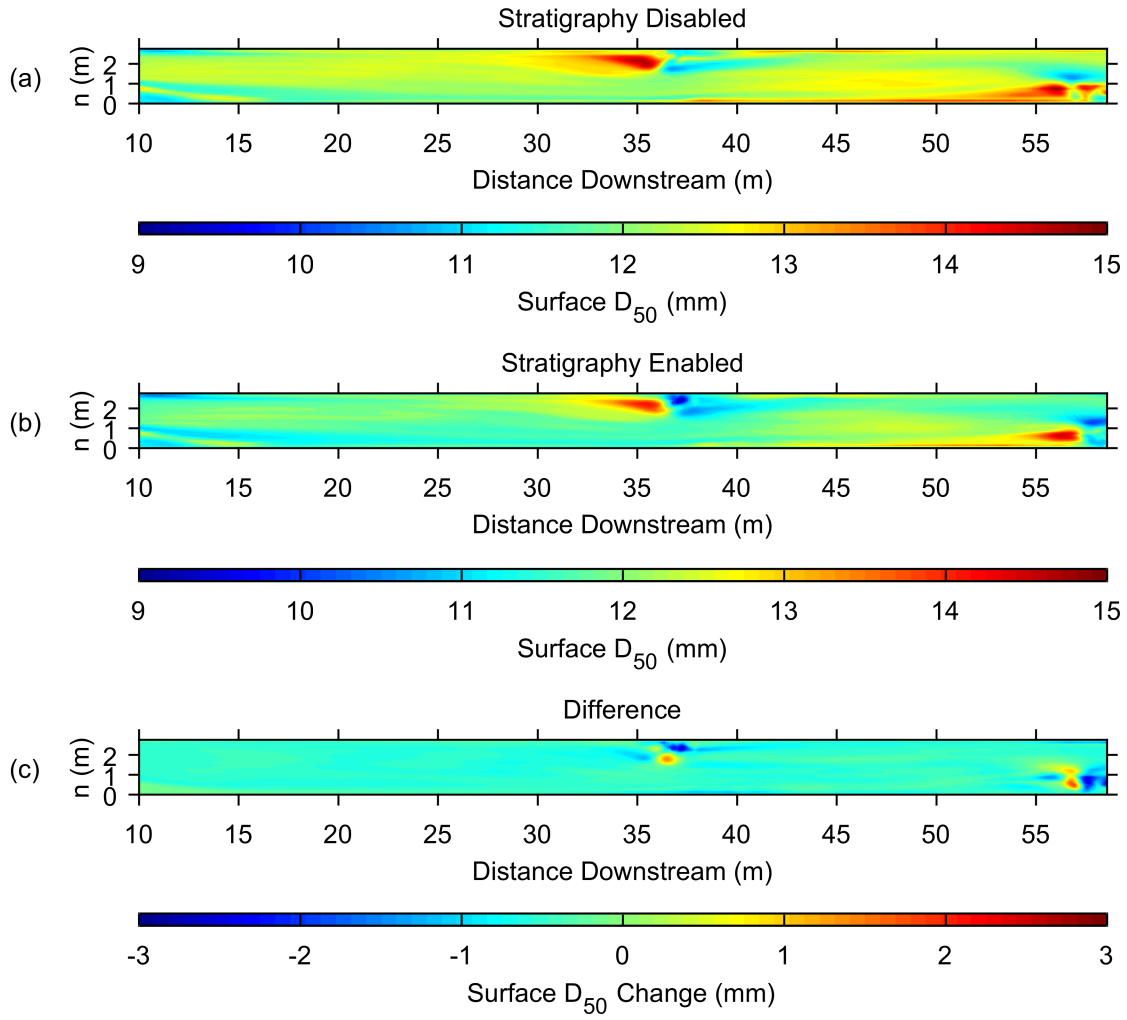

Figure 8: Surface median grain size for Scenario 1 (a) with and (b) without stratigraphy enabled. (c) Difference in surface median grain size between (a) and (b).

simulations regardless of the use of stratigraphy and the highest magnitudes are seen through each of the pools.

Stratigraphic profiles for various times during the Scenario 1 simulation are plotted in Figure 9 for the four locations A, B, C, and D (shown in Figure 6). These locations are noted on Figure 6. Location A is at a grid point in the coarse region of the bar top on the left alternate bar. Location B is the deepest region in the pool adjacent to the bar top captured at location A. Location C is an arbitrarily selected point in the middle of the channel upstream of locations A and B. Location D captures the stratigraphy of a point

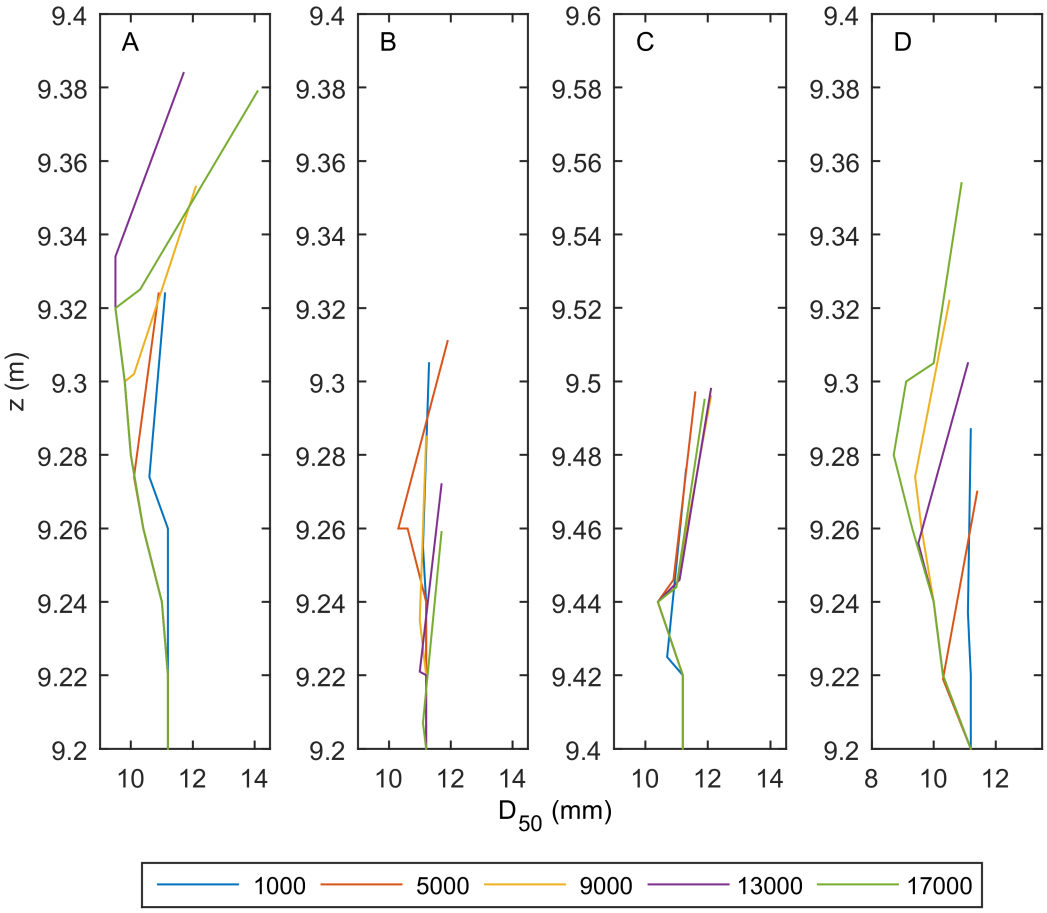

Figure 9: Stratigraphy profiles for points A, B, and C shown on Figure 6. Location A is at the coarse top of the persistent bar on channel left. Location B is the deepest point in the pool adjacent to location A. Location C is an arbitrary mid-channel point located upstream of locations A and B. Location D corresponds to the finer portion of the bar just downstream of location A. Legend values are the simulation time in seconds.

somewhat downstream of location A but still within the extent of the bar. Locations A and D have the greatest amount of vertical sorting present. Both profiles show a coarsened surface that quickly fines smaller than the initial median grain size of 11.2 mm at minimal subsurface depth. A gradual coarsening with increased depth then occurs until reaching the unmodified bulk subsurface material.

While the temporal resolution of these profiles is relatively coarse, it is still possible to gain a sense of how the stratigraphy is a feedback on the flow and sediment transport solutions. For example, at location A, the subsurface is about the same between time 13,000

s and 17,000 s but the surface has coarsened considerably. Furthermore, the stratigraphic profile is coarser at 17,000 s for the top 6 cm. Below 6 cm depth, the two profiles are identical. This indicates that a period of degradation occurred where the finer material present at 13,000 s in the subsurface was eroded away and replaced with coarser material at 17,000 s.

3.2 Scenario 2 - Stratigraphy Effects on Free Alternate Bars

In Scenario 2 a series of freely formed, migrating, alternate bars form in the 200-meter-long channel. The development and progression of these features is shown in Figure 10. The bars initially form towards the upstream end of the flume, then grow and propagate to the downstream end of the flume. Once a train of these smaller bars develops down about two thirds of the flume, their amplitude quickly increases to a size similar to the bars developed in Scenario 1. These larger bars propagate slightly downstream until reaching a state of dynamic equilibrium where a series of 5 to 6 migrating, alternate bars form at the downstream end.

As in Scenario 1, surface grain sorting displays the general pattern of coarse bar tops and fine pools as seen in Figure 11. At the beginning of the simulation, this sorting pattern happens to a small degree within the small amplitude alternate bar morphology that first develops. Sorting is most pronounced at later times in the simulation, at downstream parts of the domain where bar-pool topography has fully developed.

Figure 12 presents detrended topography for a 30-meter portion of the domain of Scenario 2 simulations run with and without stratigraphy enabled. The obvious difference between the two simulations is the downstream shift in the bar location for the stratigraphy enabled simulation. The bar front is approximately 5 meters further downstream when stratigraphy is enabled, suggesting that stratigraphic feedbacks affect bar dynamics. The shape of the bars and pools has also noticeably changed between the simulations. I noted that the bar computed with stratigraphy enabled is wider, particularly at the front, with the high point

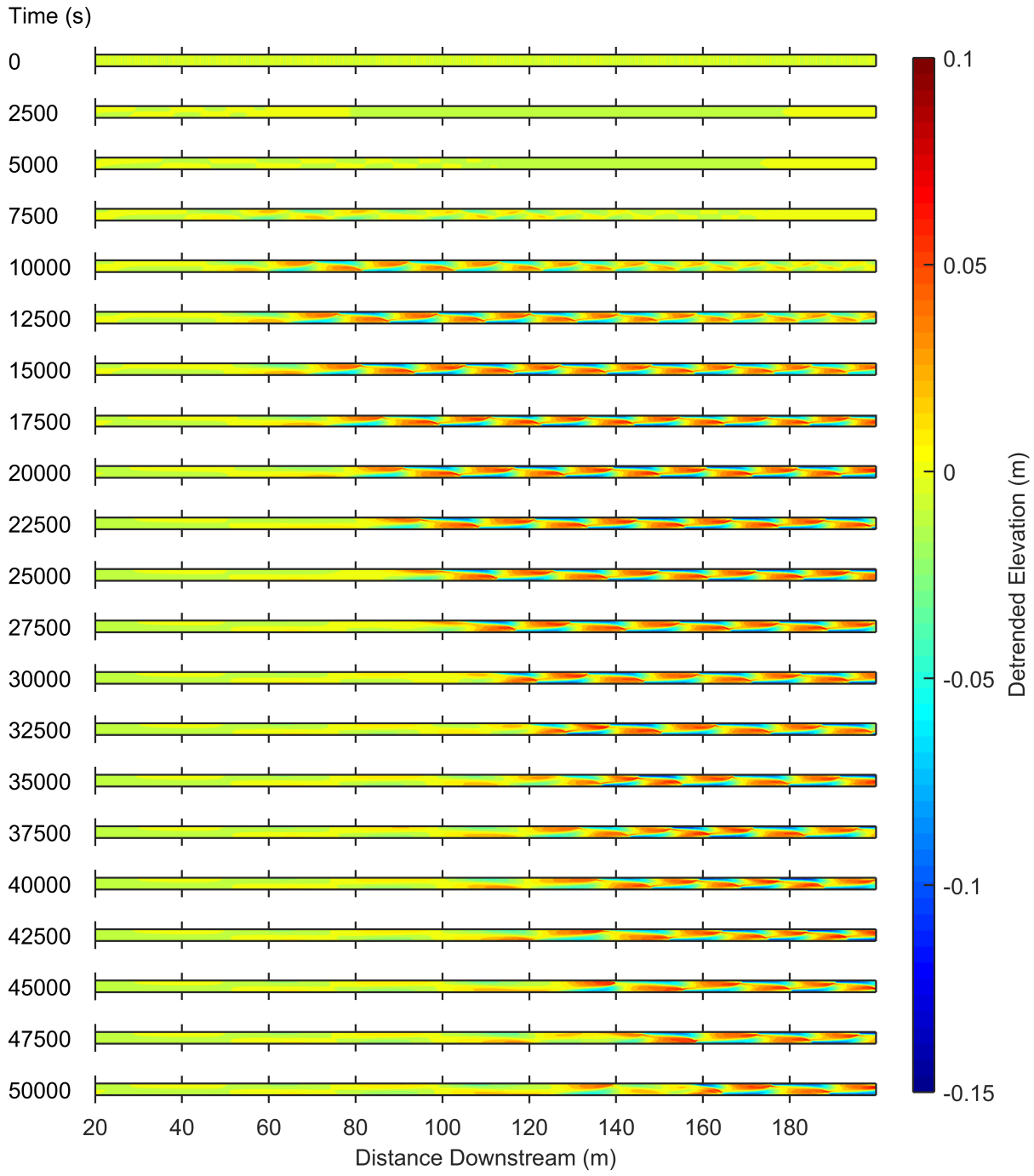

Figure 10: Detrended topography time series for Scenario 2 run with stratigraphy enabled.

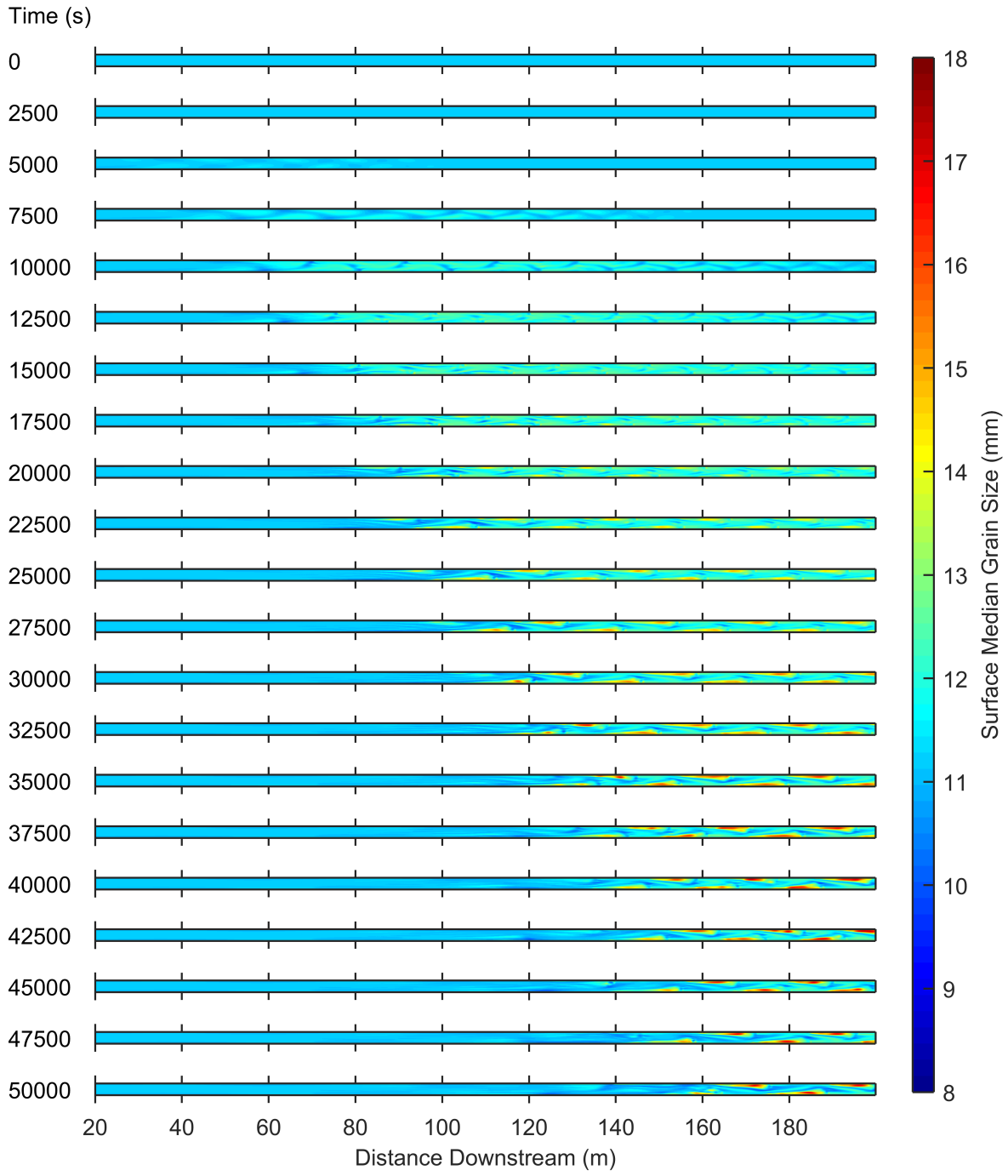

Figure 11: Surface median grain size time series for Scenario 2 with stratigraphy enabled.

more toward the center of the channel. The lee of the bar face is steeper with stratigraphy enabled as well. This ultimately shows a shorter (lengthwise) bar that is wider when stratigraphy is enabled. Also of interest is the change to the pool opposite this bar. It is clearly shorter lengthwise, but is also considerably deeper than in the simulation without stratigraphy. Overall the bar dynamics and morphology are considerably different when the model is run with stratigraphy. This is in contrast to Scenario 1 where little if any modification to the bar dynamics and morphology is observed.

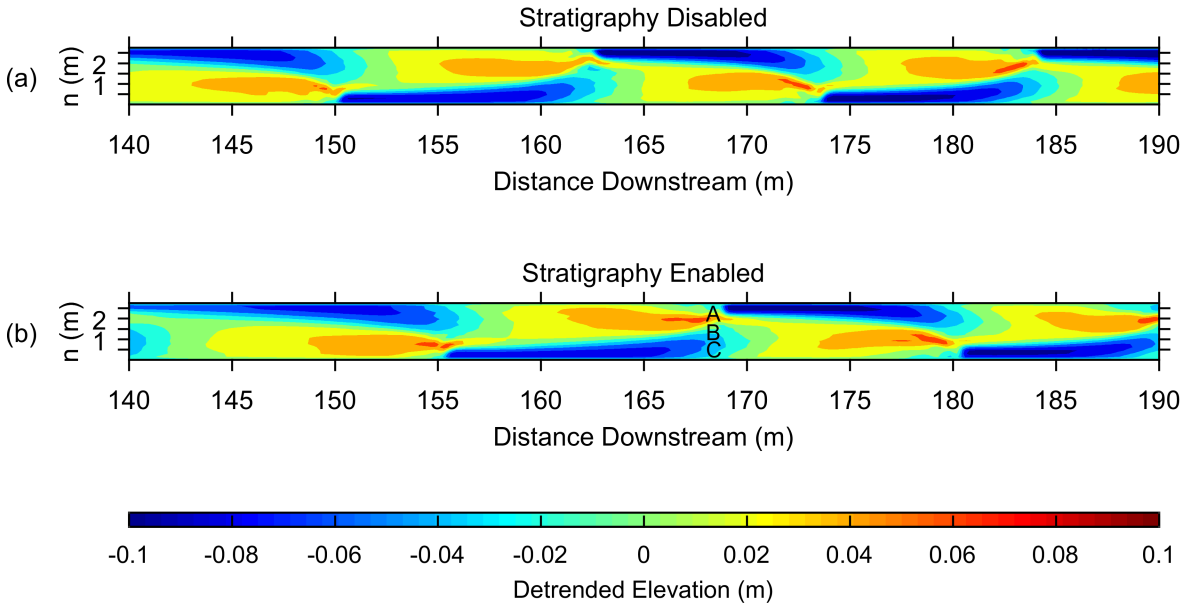

Figure 12: Scenario 2 detrended topography at time = 45,000 s for a simulation run (b) with stratigraphy enabled and one run (a) without stratigraphy. The locations A, B, and C are where stratigraphic profiles are pulled throughout the simulation.

Figure 13 shows that in Scenario 2 the degree of sorting is increased when stratigraphy is enabled. While this degree of sorting varies over the entire simulation time, I see that the pools are about 2 to 4 mm finer (depends on location in pool and each individual pool) and that the bar tops are 1 to 2 mm coarser than in the simulation without stratigraphy enabled. The change in degree of sorting when stratigraphy enabled can be observed by comparing the distribution of the median surface grain sizes between simulations run with and without stratigraphy. Histograms showing these distributions are in Figure 14. To avoid skewing the

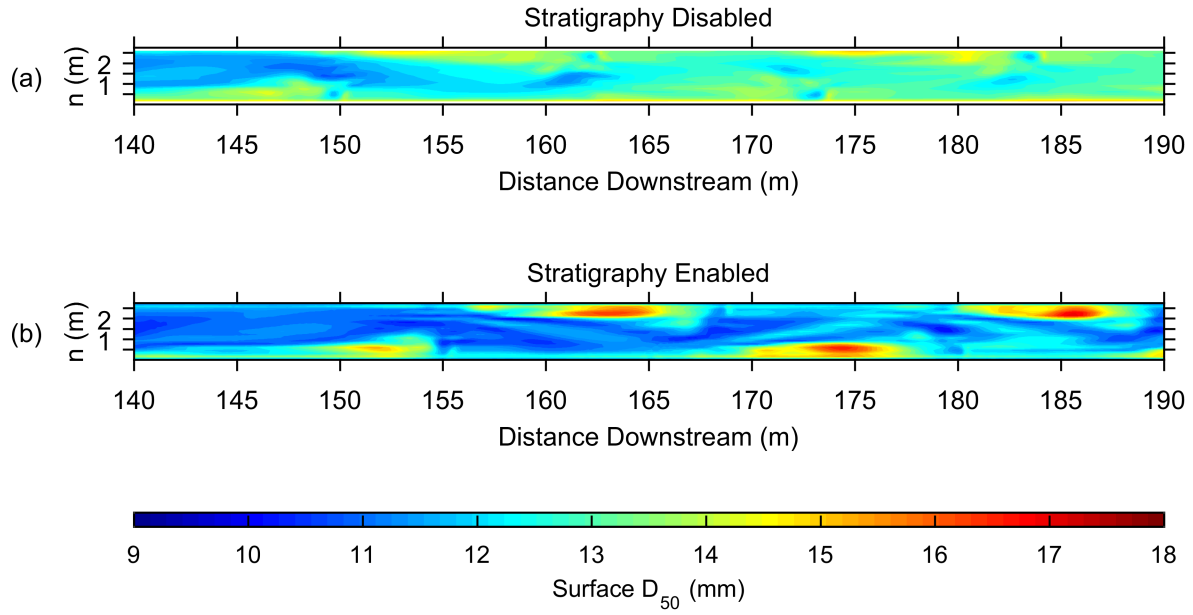

Figure 13: Median grain size at 45,000 seconds for simulations of Scenario 2 run (b) with and (a) without stratigraphy enabled. Note the considerable median grain size change compared to Figure 8.

distributions and allow detection of sorting changes within the alternate bars, the upstream unsorted region of the model domain is omitted. The sampled region encompasses the three most downstream alternate bar units. This area is not exactly equal between simulations, but generally extends from x = 130 m to the downstream boundary (a region slightly larger than that shown in Figure 13). From Figure 14 it is clear the distribution of surface median grain sizes has widened with stratigraphy enabled. This indicates that a wider range of grain sizes are present within the alternate bar morphology. To quantify the change in degree of sorting, the standard deviation from each distribution is computed. When stratigraphy is disabled, the standard deviation is 0.81 mm. With stratigraphy enabled, the standard deviation increases significantly to 1.41 mm. Levene's test confirms the significance of this change in standard deviation with a p-value much less than 0.01. This increase in standard deviation is further evidence that the degree of sorting has increased due to inclusion of stratigraphic feedbacks.

In addition to the increased degree of sorting shown in 14, it is also clearly evident that

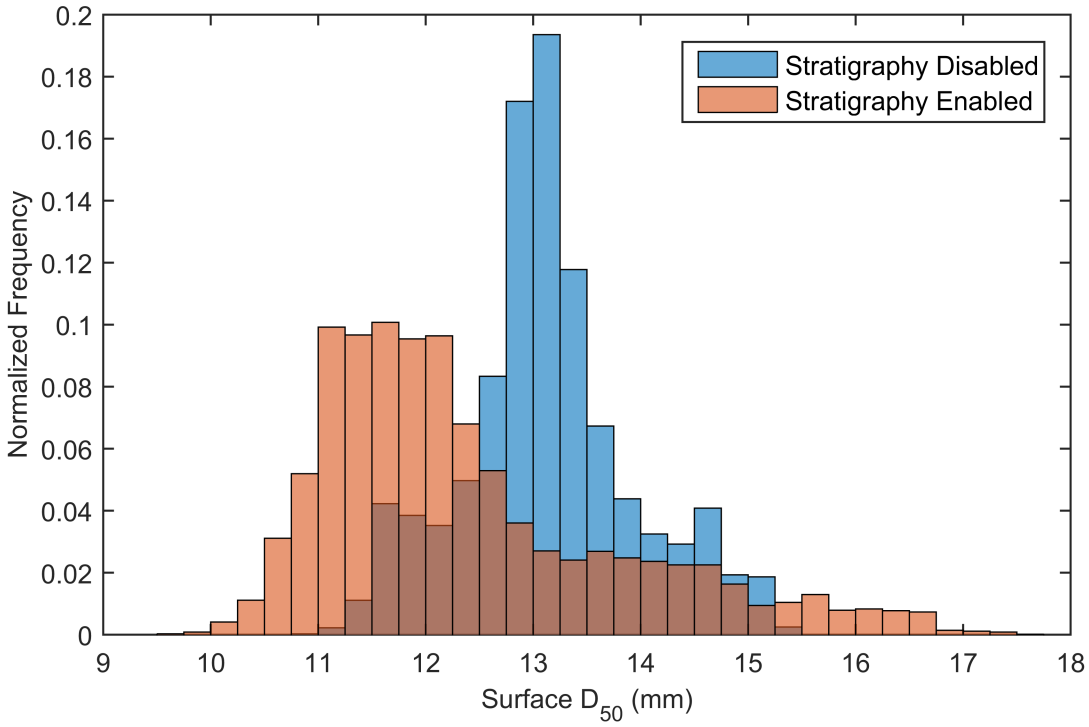

Figure 14: Distribution of surface median grain sizes for the series of 3 alternate bar units at the downstream end of the model domain at 40,000 seconds for simulations run with and without stratigraphy enabled. The frequencies have been normalized because the number of grid cells in the sampled area is different between the two simulations due to changes in bar morphodyanmics. The standard deviation is 0.81 mm without stratigraphy and 1.41 mm with stratigraphy enabled.

the overall sample region median grain size has fined. This is seen by the left shift of the stratigraphy enabled distribution. Of greatest interest however, is that there are regions with a median surface grain size finer than the initial bulk median grain size of 11.2 mm when stratigraphy has been enabled. Without stratigraphy, there are no regions with a median surface grain size smaller than 11.2 mm.

The magnitude of bedload transport rates are comparable between the two simulations. These rates are shown for time = 45,000 seconds in Figure 15. Depth is plotted above the transport rate to help with identification of bar and pool locations. It is fairly clear that in both scenarios the regions of highest transport start at the downstream end of the pools and continue downstream across the channel just along the upstream, lateral edge of the

next downstream bar. While it is somewhat difficult to directly compare the two simulations as the bars have different shapes and frequencies, there are some minor differences in the transport magnitude that may be directly attributed to including stratigraphy (opposed to indirects effects though morphological feedbacks; i.e., different shaped bars). Most notable is that the widths of the regions with high transport rates are narrower and remain focused predominately along the edge of the next downstream bar.

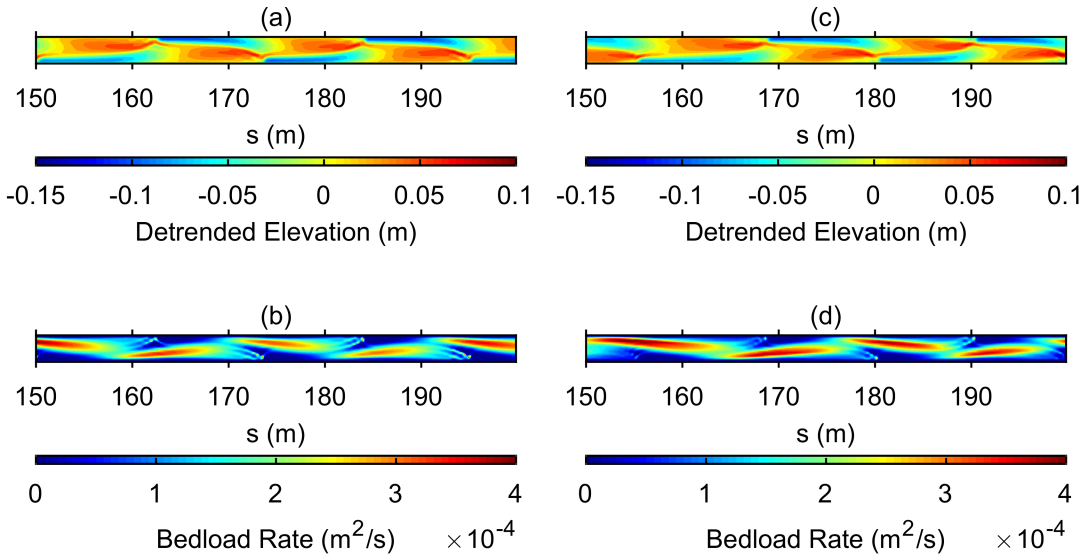

Figure 15: (a) Detrended elevation and (b) bedload transport rates for a model run without stratigraphy enabled. (c) Detrended elevation and (d) bedload transport rates for a model run with stratigraphy enabled.

To gain insight into how the stratigraphy is developed and accessed over time, stratigraphic profiles were exported at specified grid points at specific times during a simulation. These profiles are shown in Figure 16 for the three locations, A, B, and C shown in Figure 12. The points were selected towards the downstream end of the domain because the dynamic equilibrium condition consisting of migrating alternate bars is only observed in the lower third of the domain. Location A is located toward channel left in the region where the tops of migrating bars exist and generally the deepest regions of passing pools are found. Location C is located toward channel right and captures the same progression of passing bar

tops and pools as location A, just on the opposite side of the channel. Location B is in the center of the channel between locations A and C.

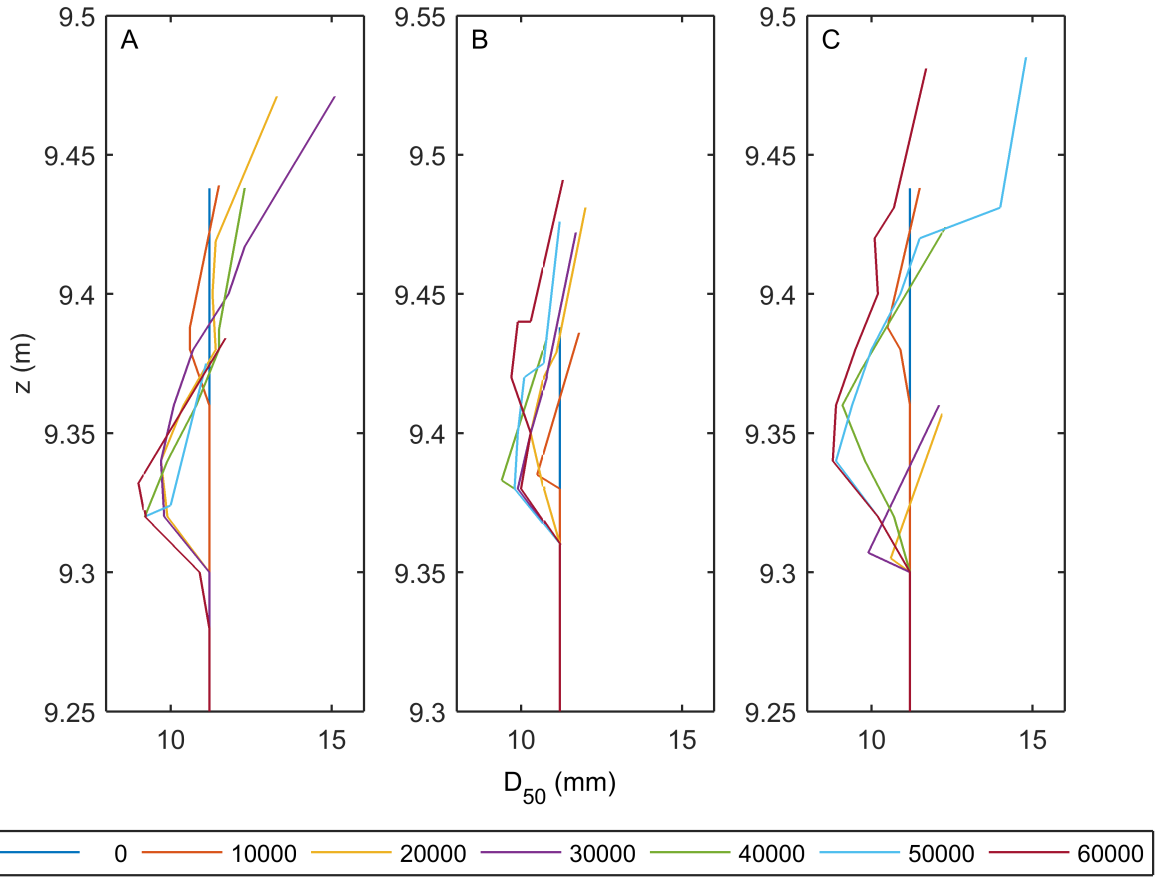

Figure 16: Time series of stratigraphic profiles for locations A, B, and C shown on Figure 12. Legend entries refer to simulation time in seconds.

In general, the same stratigraphic patterns are seen at locations A and C. This is not surprising as the migrating alternate bar morphology during equilibrium is essentially symmetric. At these side of channel locations, the development of vertical sorting is clearly evident. For the lines that reach higher elevations (z on plot), it is evident that at that time, a bar top is passing the point. At these times, the surface has coarsened which is also shown in Figure 13. However, it is seen that this coarse patch only exists near the surface and does not continue down into the bar. Beginning at 5 cm below the surface (thickness of the active layer), the median grain size is anywhere from 1 mm to 5 mm finer than the surface. The

degree of fining with depth below the surface is greatest at time 30000 seconds at location A. A similar profile is observed at location C at time 50000 seconds. In the finest regions of the profile, I noted that the finest median subsurface grain size is relatively unchanged regardless of whether a bar or pool is passing the location and the elevation of this fine layer is fairly constant.

Location B in the center of the channel shows a lesser degree of sorting compared to locations A and C. A layer finer than the surface still develops, but to a much lesser degree (only about 1 mm finer). In general though, by observing these points I documented much greater degrees of vertical sorting on the sides of the channels where more aggradation and degradation occur and only small degrees of vertical sorting mid channel.

3.3 Stratigraphic Profiles

A longitudinal profile was extracted through a single bar unit at the end dynamic equilibrium state (time = 50,000 seconds) for Scenario 2 and is shown in Figure 17. The bar unit extends from approximately 165 m to 190 meters downstream. The profile is located about 0.46 meters from the right side of the channel. Along this profile, vertical plots showing the relative grain size in the subsurface are shown approximately every 2.5 meters along the profile. Relative grain size in this plot is described by the value $\left(\frac{D_{50n}}{D_{50b}} - 1\right)$ where D_{50n} is the median grain size of the stratigraphy layer at the output time and D_{50b} is the median grain size of the initial bulk material (11.2 mm). Therefore, a value of 0 indicates that the median grain size has not changed, while negative values indicate a finer median and positive values indicate a coarser median grain size. With the exception of the top stratigraphy node, whose elevation is determined by the elevation of the bed and thickness of the local active layer, the vertical spacing of the nodes is equal to the stratigraphy layer thickness of 0.02 m.

Consistent with what has already been shown, the pools have relatively little complex vertical sorting, while the bars are considerably more complex. Furthermore, the complex vertical sorting in the bar consists of a fine layer below a coarser layer. It is clear that

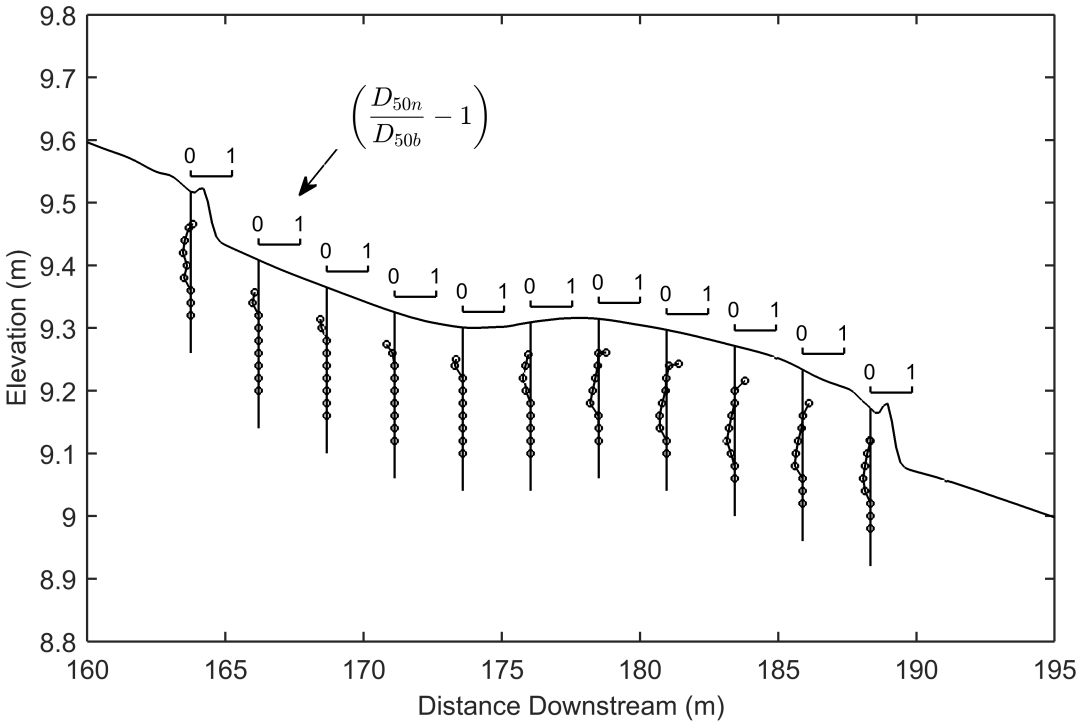

Figure 17: Longitudinal profile 0.46 meters from the right edge of the channel at 50,000 seconds through a single bar unit with stratigraphy profiles shown within the entire bar unit. Note that the value $\left(\frac{D_{50n}}{D_{50b}} - 1\right)$ is plotted on separate x-axes, however the y-axis remains the same for the stratigraphy plots and the longitudinal profile. D_{50n} = median grain size of stratigraphy layer n and D_{50b} = median grain size of initial bulk material. The location of the profile is shown in Figure 12. Plot form is from *Lanzoni* [2000].

these respective patterns are fairly consistent throughout the complete bar unit, with the exception of the very front of the bar head where the coarse layer does not exist.

4 Discussion

4.1 Stratigraphy Effects on the Degree of Sediment Sorting

As shown in both Scenario 1 and Scenario 2, the degree of sorting on the surface is greater when the model is run with stratigraphy enabled. In general, most of the coarse patches became coarser while the pools become slightly finer. This increased sorting was more present in Scenario 2 however. From the profiles in Figure 16, there is a consistently finer subsurface which is cyclically accessed as the migrating alternate bars propagate downstream. Furthermore, while the temporal resolution of the stratigraphy output is fairly coarse, it appears that the subsurface gets progressively finer after each cycle of degradation and aggradation.

As shown by *Nelson et al.* [2010] and *Nelson et al.* [2015a], the pools in straight channels with alternate bars tend to be fine-grained due to lateral size-selective transport of fine sediment off of adjacent bars. The simulations described here incorporating stratigraphy are able to preserve this fine material in the subsurface as pools aggrade during bar migration. During subsequent degradation, this stored fine material becomes exposed on the bed surface, decreasing the local hydraulic roughness. This decreased roughness increases the local velocity and shear stress, allowing for transport of coarser particles through the pool and on top of the downstream bar. Over many aggradation-degradation cycles, this leads to a bar top that is ultimately coarser than if the upstream pool was not allowed to become progressively finer through stratigraphic feedbacks.

A small degree of fining in the transition zone between pools is also seen in both scenarios. While the vertical sorting is not nearly as pronounced in these areas (location C in Figure 6 and location B in Figure 12), the stratigraphy profiles still show a small amount of fining just below the bed surface. The lower amplitude cycles of aggradation and degradation still access these finer layers which likely promote a slight fining of the bed in these regions.

4.2 Stratigraphic Signature of Migrating Alternate Bars

Comparing the two scenarios, I see that stratigraphic feedbacks had little effect in Scenario 1, while in Scenario 2 the effects of including stratigraphy are much more dramatic. Between these two scenarios, the bar morphodynamics are very different. In Scenario 1, a stationary series of two alternate bars form relatively quickly. In Scenario 2, alternate migrating bars are present even after reaching a state of dynamic equilibrium.

Looking at Scenario 1 first, picking an arbitrary stationary point and tracking the bed change, I see the point will have only aggradation or degradation. If aggradation only occurs, then complex vertical sorting *may* develop, however there will not be a subsequent period of degradation over the point for the stratigraphy to feed back on the flow and sediment fields through roughness effects and grain size availability for transport. If degradation only occurs at this point, then there is no opportunity for complex vertical sorting to develop and the bed continues to degrade into the spatially and temporally constant initial bulk grain-size distribution. The small variations between the simulations with and without stratigraphy enabled is most likely due to the short initial period where low-amplitude migrating alternate bars develop before the large fixed bars develop.

In Scenario 2, if I pick another arbitrary stationary point (though toward the downstream end to have the greatest impact), there will be periods of aggradation and degradation. As a bar passes over the point, the bed aggrades which allows the subsurface to store any stratigraphy that may develop. However, unlike in Scenario 1, a subsequent period of degradation follows after the bar passes and a pool begins to form. As the pool progresses downstream, it exhumes the previously stored stratigraphy formed by the bar. Therefore, the potentially complex stored stratigraphy can feedback on the flow and sediment fields through roughness and grain availability feedbacks.

These results agree with the logic presented in *Lanzoni* [2000]. The stratigraphy profiles for locations A and C in Figure 16 confirms this development of stratigraphy. The *Lanzoni* [2000] experiments were conducted using a variety of flow conditions to investigate bar for-

mation in the straight channel using a bimodal mixture of sand and fine gravel. In the run named P2009, he notes that a train of migrating alternate bars and the associated process of scour and fill during the initial phase of the experiment may result in strong vertical sorting. To investigate this, he maps a longtitudinal profile through a bar unit and plots the stratigraphy through the bar unit in a manner very similar to that previously shown here in Figure 17. This result from the *Lanzoni* [2000] experiment is shown below (Figure 18).

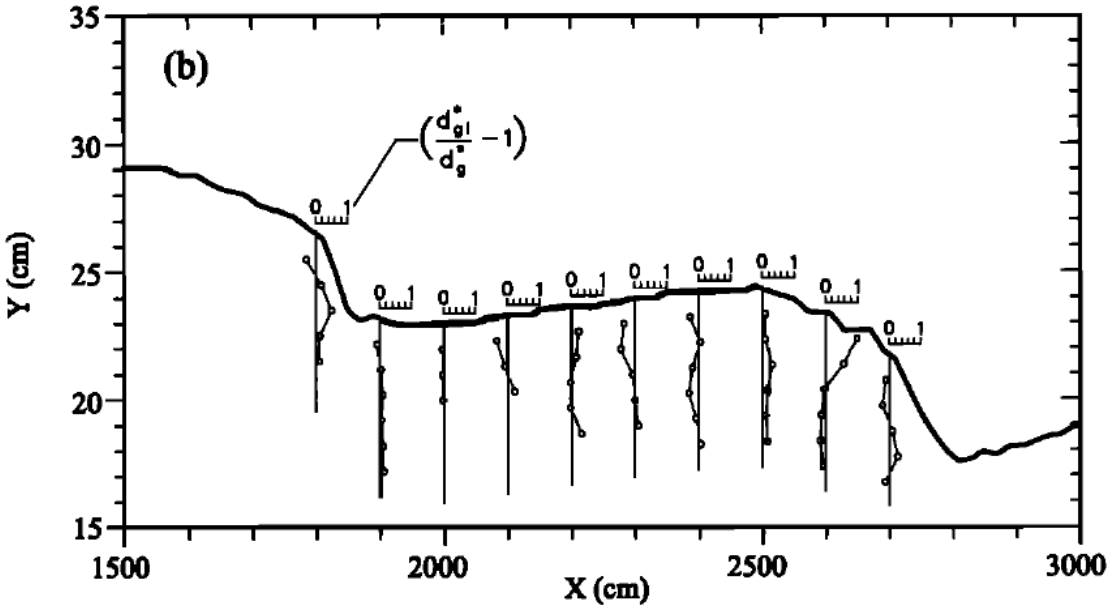

Figure 18: Longitudinal profile with stratigraphy profiles through a single bar unit from the experiment P2009 in the *Lanzoni* [2000] study (Figure 7b in his paper). This figure reports the ratio of subsurface geometric mean grain size to initial bulk geometric mean grain size less 1, while our results in Figure 17 report the ratio of median grain sizes less 1.

While direct comparison of our Scenario 2 results with the Lanzoni P2009 experiment results cannot be made due to many differences (flume geometry, water discharge, sediment grain-size distribution, and initial bed slope to name a few), it is difficult to ignore the similar vertical sorting patterns between my results and the Lanzoni results. Through the bar trough (pool at about 1,800 cm), both the experiment results and my simulation show a slight fining of the subsurface immediately below the bed with an essentially unchanged substrate and greater depths below the surface. Additionally, I see that the model predicts a slightly coarsened subsurface under the bar top and towards the bar head, which is also

consistent with the general pattern measured by *Lanzoni* [2000]. Additionally, the bar heads from both results show a slightly fined subsurface. It is important to stress that these are only qualitative observations of the general trend in sorting through the bar units. Beyond the dissimilarities in initial conditions, the results from Lanzoni report the ratio of geometric mean grain size and not the median grain size as was reported in Figure 17.

4.3 Stratigraphy Effects on Bar Morphology and Dynamics

In Scenario 2 I noted that the alternate bars are predicted to be slightly wider when the model is run with stratigraphy enabled (Figure 12). The widening indicates that subsurface stratigraphy can have a considerable effect on the morphology of the bars. While the widening is likely attributed to several feedback mechanisms, it could be mostly attributed to the fining of the pools allowed when stratigraphy is used (Figure 13). Fining within the pools allows for a slightly contracted zone of high sediment transport rates clearly seen in in Figure 15. Because the primary bedload transport zone is narrowed when stratigraphy is accessed, the bars can become wider. Note that in Figure 15, due to a change in bar dynamics due to the inclusion of stratigraphy, similar bars are located at different points in the channel, so in order to compare the same transport zones between the two runs, it is necessary to locate similar bars from the detrended elevation plots.

Bar amplitude can be examined by comparing the difference elevation from a bar top and the adjacent pool. This is shown in Figure 19 for simulations run with and without stratigraphy. While subtle, I see that the amplitude of the bars is increased when stratigraphy is enabled. Additionally, the wavelength if slightly shortened with stratigraphy enabled. The change in wavelength is potentially due to the change in bar dynamics discussed later in this section. The cause behind the increase in bar amplitude follows along the reasoning for the increase in bar width when stratigraphy is enabled. From Figure 12, the elevation of the bar tops remain roughly the same with or without stratigraphy. The pools, however, are lower by 1 to 2 cm when using stratigraphy. This is confirmed by extracting the cross sections

shown in Figure 20. This greater amount of degradation can be attributed to the finer pool surface which allows for increased sediment transport pool to pool. Therefore, the increase in bar amplitude observed in Figure 19 when using stratigraphy is due to the increased depth of the pool adjacent to each bar top.

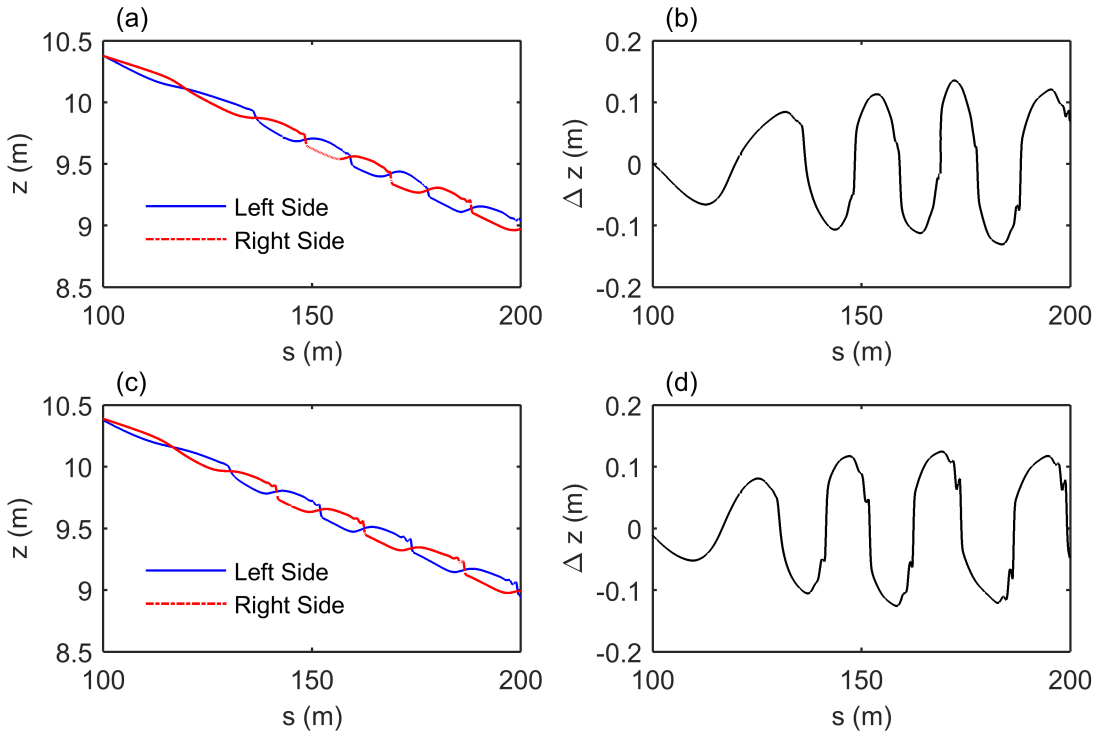

Figure 19: (a and c) Bed profiles pulled 46 cm from the left and right sides of the channel where panel (a) is for a run with stratigraphy and panel (c) is a run without stratigraphy. (b and d) Difference in elevation between the right and left profiles. All plots are for a simulation time of 40,000 seconds.

Bar dynamics are also modified when stratigraphy is included in the model. Some of the previous results hint at this (Figure 12 for example), though how the dynamics have changed is not entirely clear. To look into this, longitudinal profiles are extracted at 5,000 second intervals about 50 cm from the right edge of the channel. They are plotted as a time series for a run without stratigraphy and a run with stratigraphy enabled in Figures 21 and 22 respectively. Tracking the front of the bars as they propagate downstream and noting the downstream distance for each time allows for calculation of the bar celerity which is shown

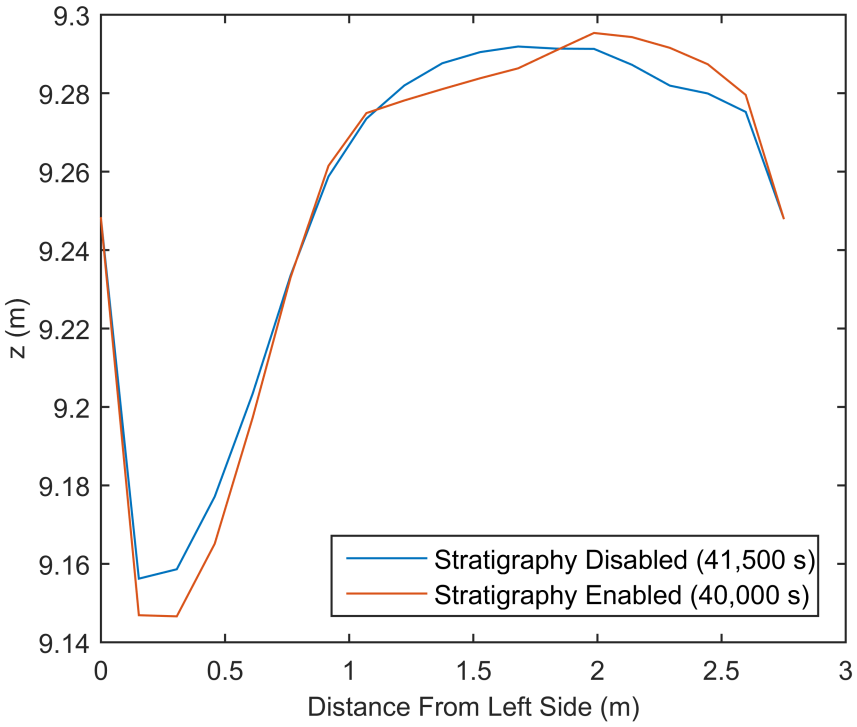

Figure 20: Cross sections extracted 181.89 meters downstream. The section for stratigraphy disabled is at a later time to capture the same location in the pool-bar sequence as was captured for the stratigraphy enabled profile.

by the diagonal black line over each plot. The inverse slope of this line is the bar celerity (a more vertical line indicates slower bar movement). From these two plots I see that when stratigraphy is enabled, the bar celerity is increased by about 1 cm/min. Additionally, the bar celerity is fairly constant and does not speed up or slow down for either simulation.

How exactly the stratigraphy is causing this slight increase in bar celerity is up for speculation. It could be attributed the greater degree of surface sorting observed when stratigraphy is enabled. The coarser bar tops are rougher and would see a slight decrease in velocity and shear stress. The pools would see the opposite, with a higher velocity and shear stress. If the erosion or propagation of the bars is more controlled by the erosion of the pool into the next downstream bar, the increased degradation in the pool my be pushing the next downstream bar slightly downstream.

While no direct validation of the stratigraphy framework against a flume study is con-

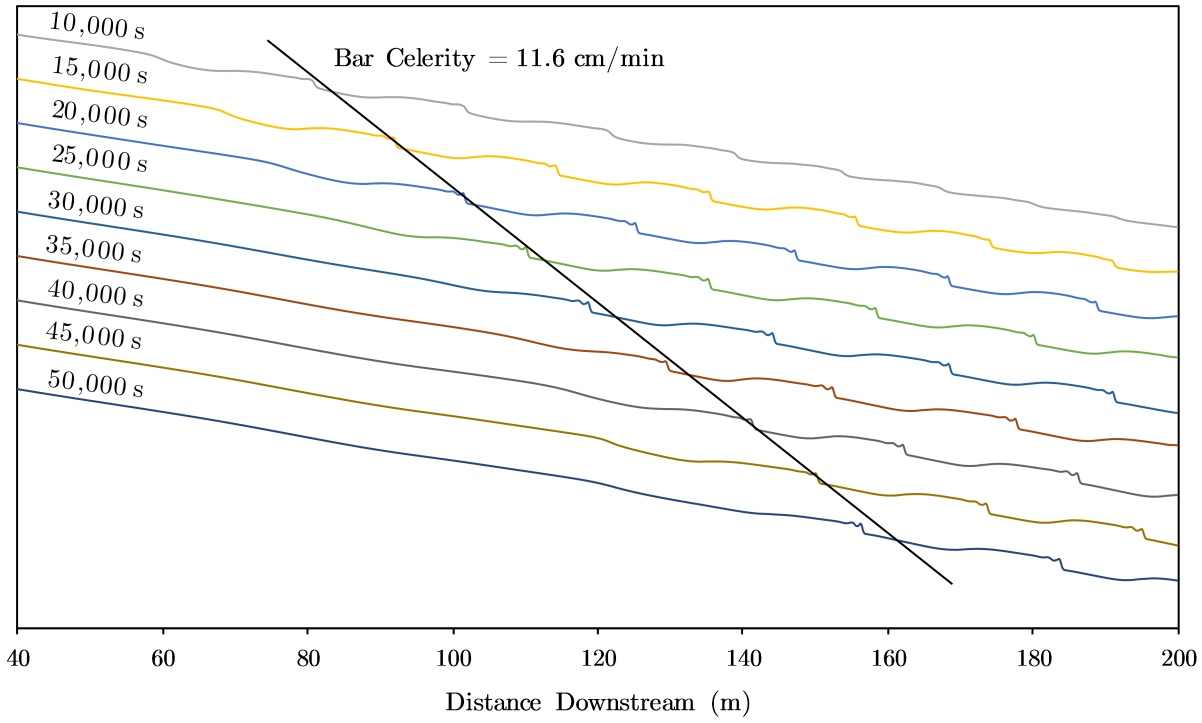

Figure 21: Longitudinal profiles extracted about 50 cm from the right channel edge from a simulation with stratigraphy disabled. The front of the bars are tracked through time to calculate a bar celerity of approximately 11.6 $^{\text{cm}}/_{\text{min}}$.

ducted here, some results point to the framework allowing the model to better simulate conditions observed in a flume. In both Scenario 1 and Scenario 2, the overall degree of sorting of the bed surface increased (coarse bar tops are coarsened, fine pools become finer) when the stratigraphy framework was used. It was noted by *Nelson et al.* [2015a] that the lack of stratigraphy storage may be a reason for their model predicting smaller degrees of sorting when compared against flume studies. In particular, accounting for stratigraphy allows the model to predict surface patches finer than the bulk distribution (Figure 14), which the *Nelson et al.* [2015a] model could not do. Given the higher degrees of sorting with stratigraphy enabled, it is promising that the framework is allowing the model to more closely simulate conditions observed in the lab and in rivers undergoing periods of aggradation and degradation due to land use change or flow regulation for example.

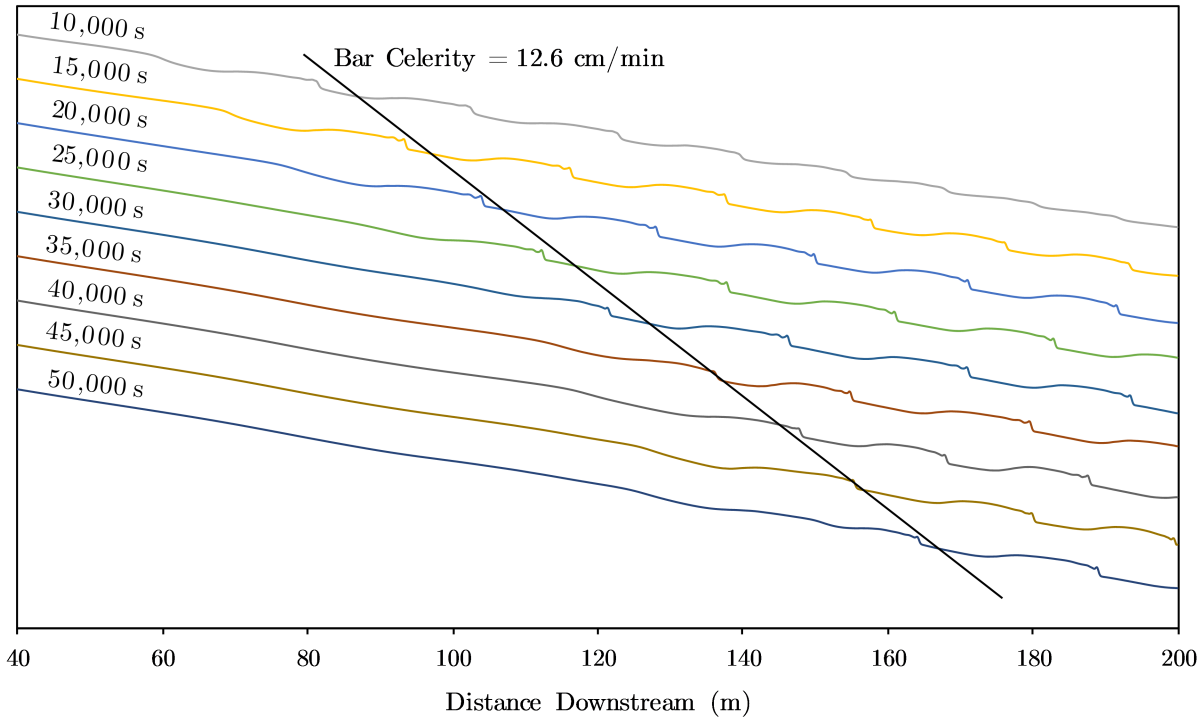

Figure 22: Longitudinal profiles for various simulation times extract about 50 cm from the right channel edge from a simulation with stratigraphy enabled. The front of the bars are tracked through time to calculate a bar celerity of approximately 12.6 $^{\text{cm}}/_{\text{min}}$.

5 Conclusions

A stratigraphy framework has been integrated into the 2D morphodyanmic model FaST-MECH which allows for the creation, storage, and access of potentially complex vertical heterogneity in the subsurface. From the two scenarios presented it is clear that the case of freely migrating alternate bars (Scenario 2) produces a stratigraphic signature due to local aggradation-degradation cycles. The forced bars simulated in Scenario 1 are not dynamically migrating, so stratigraphy is less important and has less of an effect on bar morphology or surface sorting.

The stratigraphic signature of migrating bars in Scenario 2 was found to consist of a slightly fined subsurface within pools and a coarser layer over a finer layer within the pools. Accessing the fine subsurface layers during degradation periods allowed for greater degrees of sorting in terms of coarser bar tops and finer pools. This change in sediment sorting was found to have impacts on both the bar morphology and, to a lesser extent, bar dynamics. Increased transport pool-to-pool creates wider bars, larger bar amplitudes through deepening of pools, and slightly faster movement of bars through the channel.

The increased degree of sediment sorting observed in both scenarios suggests that including stratigraphy in the model improves the model's ability to predict sorting and ultimately has closer to match to observed experimental results. Comparisons of Scenario 1 results with the flume experiment in *Nelson et al.* [2015a] show that the model predicts grain size within the pools more accurately. Furthermore, the overall greater spread of grain sizes represented on the bed in both Scenario 1 and 2 suggest that increased degrees of sorting can be achieved with the use of a stratigraphy framework. This supports the *Nelson et al.* [2015a] hypothesis that decreased degrees of sorting were predicted due to lack of stratigraphy creation, storage, and access.

The stratigraphy framework was coded in Fortran, which is likely not the most efficient language in which to develop this framework. Dynamic allocation in Fortran is not feasible,

therefore the stratigraphy routine is memory-intensive as a very large 3D space of stratigraphy nodes needs to be preallocated. Around half of these nodes contain no information and are filling memory unnecessarily. Programing and compiling the stratigraphy framework in a language which allows for dynamic allocation of memory could make the stratigraphy framework implemented much more efficient computationally.

This study focused on the fairly simple conditions of steady flow, no net aggradation and degradation, and a straight channel. A logical progression into the study of stratigraphy would be relaxing some or all of these conditions. The effects of sediment supply in alternate bar morphologies are still not fully understood and from the experiments by *Bankert* [2016], it is clear that stratigraphy can be important. Including the ability to modify the upstream sediment supply would allow for more detailed modeling of these potentially important feedbacks. Furthermore, due to the reversal of grain size sorting patterns in meandering channels (coarse pools and fine bar tops), the development of stratigraphic signatures and the associated feedback mechanisms could be notably different.

From this study, I have shown that stratigraphy is conditionally important in that aggradation is needed to develop vertical sorting and degradation is needed to access the stored subsurface deposits. Therefore, stratigraphy will play an important role in systems with migrating alternate bars, but at the same time it would likely have important effects in systems with widespread aggradation followed by degradation. Modeling efforts for these types of conditions could be largely flawed if stratigraphic effects are not accounted for. Furthermore, I have shown that stratigraphy can impart some influence on the sorting patterns observed in a channel. Better prediction of these sorting patterns ultimately improves our ability to predict river channel evolution. The improved ability to predict channel evolution and the associated improved understanding of river mechanics ultimately has important implications for a host of applications in fluvial geomorphology and river engineering. For example, as habitat restoration with an emphasis on fish species becomes increasingly popular and important, the ability to predict locations of specific sized gravels for spawning becomes an

important tool in being able to design and fund restoration projects. Additionally, while supply effects were not examined here, a better understanding of stratigraphy feedbacks could be crucial in understanding and analyzing real systems that have undergone aggradation and degradation due to sediment supply changes due to activities such as dam construction and/or removal, gravel augmentation, and logging.

6 References

Ashida, K., and M. Michiue (1972), Study on hydraulic resistance and bed-load transport rate in alluvial streams, in *Proceedings of the Japan Society of Civil Engineers*, 206, pp. 59–69, Japan Society of Civil Engineers.

Bankert, A. (2016), Alternate bar dynamics in response to increases and decreases of sediment supply, Master's thesis, Colorado State University.

Bluck, B. (1971), Sedimentation in the meandering river endrick, *Scottish Journal of Geology*, *7*(2), 93–138.

Bridge, J. S., and J. Jarvis (1976), Flow and sedimentary processes in the meandering river south esk, glen clova, scotland, *Earth Surface Processes and Landforms*, *1*(4), 303–336.

Buffington, J. M., and D. R. Montgomery (1999), A procedure for classifying textural facies in gravel-bed rivers, *Water Resources Research*, *35*(6), 1903–1914, doi:10.1029/1999WR900041.

Clayton, J. A. (2010), Local sorting, bend curvature, and particle mobility in meandering gravel bed rivers, *Water Resources Research*, *46*(2), n/a–n/a, doi:10.1029/2008WR007669, w02601.

Crowder, D. W., and P. Diplas (1997), Sampling heterogeneous deposits in gravel-bed streams, *Journal of Hydraulic Engineering*, *123*(12), 1106–1117.

Cui, Y., C. Braudrick, W. E. Dietrich, B. Cluer, and G. Parker (2006), Dam removal express assessment models (dream) part 2: Sample runs/sensitivity tests, *Journal of Hydraulic Research*, *44*(3), 308–323.

Dietrich, W. E., and P. Whiting (1989), Boundary shear stress and sediment transport in river meanders of sand and gravel, in *River Meandering*, edited by S. Ikeda and G. Parker, pp. 1–50, American Geophysical Union, Washington, D.C.

Dietrich, W. E., J. W. Kirchner, H. Ikeda, and F. Iseya (1989), Sediment supply and the development of the coarse surface layer in gravel-bedded rivers, *Nature*, *340*(6230), 215–217.

Dietrich, W. E., P. A. Nelson, E. Yager, J. G. Venditti, M. P. Lamb, and L. Collins (2005), Sediment patches, sediment supply, and channel morphology, in *4th Conference on River, Coastal, and Estuarine Morphodynamics*, edited by G. Parker and M. H. Garcia.

Ferrer-Boix, C., and M. A. Hassan (2014), Influence of the sediment supply texture on morphological adjustments in gravel-bed rivers, *Water Resources Research*, *50*(11), 8868–8890.

Garcia, C., J. B. Laronne, and M. Sala (1999), Variable source areas of bedload in a gravel-bed stream, *Journal of Sedimentary Research*, *69*(1).

Hey, R. D. (1979), Flow resistance in gravel-bed rivers, *Journal of the Hydraulics Division*, *105*(4), 365–379.

Hirano, M. (1971), River-bed degradation with armoring, in *Proceedings of the Japan Society of Civil Engineers*, 195, pp. 55–65, Japan Society of Civil Engineers.

Hoey, T. B., and R. Ferguson (1994), Numerical simulation of downstream fining by selective transport in gravel bed rivers: Model development and illustration, *Water resources research*, *30*(7), 2251–2260.

Lanzoni, S. (2000), Experiments on bar formation in a straight flume: 1. Uniform sediment, *Water Resources Research*, *36*(11), 3337–3349, doi:10.1029/2000WR900160.

Laronne, J. B., C. Garcia, and I. Reid (2000), Mobility of patch sediment in gravel bed streams: Patch character and its implications for bedload, in *Gravel-Bed Rivers V*, edited by M. P. Mosley, pp. 249–290, New Zealand Hydrol. Soc.

Legleiter, C. J. (2014), A geostatistical framework for quantifying the reach-scale spatial structure of river morphology: 2. application to restored and natural channels, *Geomorphology*, *205*, 85–101.

Lisle, T. E., and M. A. Madej (1992), Spatial variation in armouring in a channel with high sediment supply, in *Dynamics of Gravel-bed Rivers*, edited by P. Billi, R. D. Hey, C. R. Thorne, and P. Tacconi, pp. 277–293, John Wiley and Sons.

Lisle, T. E., H. Ikeda, and F. Iseya (1991), Formation of stationary alternate bars in a steep channel with mixed-size sediment: A flume experiment, *Earth Surface Processes and Landforms*, *16*(5), 463–469.

Lisle, T. E., F. Iseya, and H. Ikeda (1993), Response of a channel with alternate bars to a decrease in supply of mixed-size bed load: A flume experiment, *Water Resources Research*, *29*(11), 3623–3629.

Mosley, M., and D. Tindale (1985), Sediment variability and bed material sampling in gravel-bed rivers, *Earth Surface Processes and Landforms*, *10*(5), 465–482.

Nelson, J. M., and R. R. McDonald (1995), Mechanics and modeling of flow and bed evolution in lateral separation eddies, *U.S. Geological Survey Grand Canyon Monitoring and Restoration Center, Flagstaff, Arizona*.

Nelson, P. A., J. G. Venditti, W. E. Dietrich, J. W. Kirchner, H. Ikeda, F. Iseya, and L. S. Sklar (2009), Response of bed surface patchiness to reductions in sediment supply, *Journal of Geophysical Research: Earth Surface*, *114*(F2).

Nelson, P. A., W. E. Dietrich, and J. G. Venditti (2010), Bed topography and the development of forced bed surface patches, *Journal of Geophysical Research: Earth Surface*, *115*(4), 1–19, doi:10.1029/2010JF001747.

Nelson, P. A., D. Bellugi, and W. E. Dietrich (2014), Delineation of river bed-surface patches by clustering high-resolution spatial grain size data, *Geomorphology*, *205*, 102–119.

Nelson, P. A., R. R. McDonald, J. M. Nelson, and W. E. Dietrich (2015a), Coevolution of bed surface patchiness and channel morphology: 1. Mechanisms of forced patch formation, *Journal of Geophysical Research F: Earth Surface*, *120*(9), 1687–1707, doi: 10.1002/2014JF003428.

Nelson, P. A., R. R. McDonald, J. M. Nelson, and W. E. Dietrich (2015b), Coevolution of bed surface patchiness and channel morphology: 2. Numerical experiments, *Journal of Geophysical Research F: Earth Surface*, *120*(9), 1708–1723, doi:10.1002/2014JF003429.

Parker, G. (1990), Surface-based bedload transport relation for gravel rivers, *Journal of hydraulic research*, *28*(4), 417–436.

Parker, G. (1991), Selective sorting and abrasion of river gravel. i: Theory, *Journal of Hydraulic Engineering*, *117*(2), 131–147.

Parker, G. (1992), Some random notes on grain sorting, in *Proceeding of the Internation Grain Sorting Seminar, October 21 - 26, 1991, Centro Stefano Franscini, Monte Verità, Ascona, Switzerland*, edited by O. Vischer.

Parker, G. (2008), Transport of gravel and sediment mixtures, *Sedimentation Engineering: Processes, Measurements, Modeling, and Practice*, *110*, 165–252.

Parker, G., and E. Andrews (1985), Sorting of bed load sediment by flow in meander bends, *Water Resources Research*, *21*(9), 1361–1373.

Parker, G., C. Paola, and S. Leclair (2000), Probabilistic exner sediment continuity equation for mixtures with no active layer, *Journal of Hydraulic Engineering*, *126*(11), 818–826.

Peng, H., Z.-x. Cao, G. Pender, and H.-h. Liu (2014), Numerical modelling of riverbed grain size stratigraphic evolution, *International Journal of Sediment Research*, *29*(3), 329–343.

Scheingross, J. S., E. W. Winchell, M. P. Lamb, and W. E. Dietrich (2013), Influence of bed patchiness, slope, grain hiding, and form drag on gravel mobilization in very steep streams, *Journal of Geophysical Research: Earth Surface*, *118*(2), 982–1001.

Seal, R., C. Paola, G. Parker, J. B. Southard, and P. R. Wilcock (1997), Experiments on downstream fining of gravel: I. narrow-channel runs, *Journal of Hydraulic Engineering*, *123*(10), 874–884.

Smith, J. D., and S. R. Mclean (1984), A Model for Flow in Meandering Streams, *Water Resources Research*, *20*(9), 1301–1315, doi:10.1029/WR020i009p01301.

Toro-Escobar, C. M., C. Paola, and G. Parker (1996), Transfer function for the deposition of poorly sorted gravel in response to streambed aggradation, *Journal of Hydraulic Research*, *34*(1), 35–53.

Toro-Escobar, C. M., C. Paola, G. Parker, P. R. Wilcock, and J. B. Southard (2000), Experiments on downstream fining of gravel. ii: Wide and sandy runs, *Journal of Hydraulic Engineering*, *126*(3), 198–208.

Viparelli, E., O. E. Sequeiros, A. Cantelli, P. R. Wilcock, and G. Parker (2010), River morphodynamics with creation/consumption of grain size stratigraphy 2: numerical model, *Journal of Hydraulic Research*, *48*(6), 727–741, doi:10.1080/00221686.2010.526759.

Viparelli, E., D. Gaeuman, P. Wilcock, and G. Parker (2011), A model to predict the evolution of a gravel bed river under an imposed cyclic hydrograph and its application to the Trinity River, *Water Resources Research*, *47*(2), 1–22, doi:10.1029/2010WR009164.

Whiting, P. J., and W. E. Dietrich (1990), Boundary shear stress and roughness over mobile alluvial beds, *Journal of Hydraulic Engineering*, *116*(12), 1495–1511.

Whiting, P. J., and W. E. Dietrich (1991), Convective accelerations and boundary shear stress over a channel bar, *Water Resources Research*, *27*(5), 783–796.

Wiberg, P. L., and J. D. Smith (1991), Velocity distribution and bed roughness in high-gradient streams, *Water Resources Research*, *27*(5), 825–838.

Wilcock, P. R. (1996), Estimating local bed shear stress from velocity observations, *Water Resources Research*, *32*(11), 3361–3366.

Wilcock, P. R., and J. C. Crowe (2003), Surface-based transport model for mixed-size sediment, *Journal of Hydraulic Engineering*, *129*(2), 120–128.

Yager, E., J. Turowski, D. Rickenmann, and B. McArdell (2012), Sediment supply, grain protrusion, and bedload transport in mountain streams, *Geophysical Research Letters*, *39*(10).

Yager, E. M., J. W. Kirchner, and W. E. Dietrich (2007), Calculating bed load transport in steep boulder bed channels, *Water Resources Research*, *43*(7), 1–24, doi:10.1029/2006WR005432.

7 Appendix

7.1 Mixed-Grain-Size FaSTMECH Model

7.1.1 Hydrodynamic Model

FaSTMECH solves the vertically averaged steady-state equations of fluid mass and momentum in a curvilinear orthogonal coordinate system as derived by *Smith and Mclean* [1984]. As stated by *Nelson and McDonald* [1995] and *Nelson et al.* [2015a], correlations between velocity components are ignored as they have minimal effect on the solution for the simple river flows that FaSTMECH is designed to model. The system of three partial differential equations describing these conditions are given by Equations 5 through 7 below.

$$\frac{1}{1-N}\frac{\partial}{\partial s}\left(\langle u\rangle h\right) - \frac{\langle v\rangle h}{(1-N)R} + \frac{\partial}{\partial n}\left(\langle v\rangle h\right) = 0 \tag{5}$$

$$\begin{aligned}\frac{1}{1-N}\frac{\partial}{\partial n}\left(\langle u\rangle^2 h\right) + \frac{\partial}{\partial n}\left(\langle u\rangle\langle v\rangle h\right) - \frac{2\langle u\rangle\langle v\rangle h}{(1-N)R} = -\frac{gh}{1-N}\frac{\partial E}{\partial s} \\ +\frac{1}{\rho}\left[\frac{1}{1-N}\frac{\partial}{\partial s}\left(\langle\tau_{ss}\rangle h\right) + \frac{\partial}{\partial n}\left(\langle\tau_{ns}\rangle h\right) - \frac{2\langle\tau_{ns}\rangle h}{(1-N)R}\right] \\ +\frac{1}{\rho}\left[-\left(\tau_{zs}\right)_b + \frac{1}{1-N}\left(\tau_{ss}\right)_b\frac{\partial\eta}{\partial s} + \left(\tau_{ns}\right)_b\frac{\partial\eta}{\partial n}\right]\end{aligned} \tag{6}$$

$$\begin{aligned}\frac{1}{1-N}\frac{\partial}{\partial s}\left(\langle u\rangle\langle v\rangle h\right) + \frac{\partial}{\partial n}\left(\langle v\rangle^2 h\right) - \frac{\left(\langle u\rangle^2 - \langle v\rangle^2\right)h}{(1-N)R} = -\frac{gh}{1-N}\frac{\partial E}{\partial n} + \\ +\frac{1}{\rho}\left[\frac{1}{1-N}\frac{\partial}{\partial s}\left(\langle\tau_{ns}\rangle h\right) + \frac{\partial}{\partial n}\left(\langle\tau_{nn}\rangle h\right) - \frac{\langle\tau_{ss}-\tau_{nn}\rangle h}{(1-N)R}\right] \\ +\frac{1}{\rho}\left[-\left(\tau_{zn}\right)_b + \frac{1}{1-N}\left(\tau_{ns}\right)_b\frac{\partial\eta}{\partial s} + \left(\tau_{nn}\right)_b\frac{\partial\eta}{\partial n}\right]\end{aligned} \tag{7}$$

where s and n are the stream-wise and cross-stream coordinates respectively; R is the radius of curvature along the centerline of the channel; N is a metric accounting for the curvilinear system; $\langle u\rangle$ and $\langle v\rangle$ are stream-wise and cross-stream depth-averaged velocities; h is the flow

depth; g is the acceleration due to gravity; E is the water surface elevation; η is the bed elevation; and $(\tau_{ss})_b$, $(\tau_{nn})_b$, $(\tau_{ns})_b$, $(\tau_{zs})_b$, and $(\tau_{ns})_b$ are the shear stresses at the bed. The depth-averaged components of the Reynolds stress tensor are

$$\tau_{ss} = 2\rho K \left(\frac{1}{1-N} \frac{\partial u}{\partial s} - \frac{v}{(1-N)\, R} \right) \tag{8}$$

$$\tau_{nn} = 2\rho K \frac{\partial v}{\partial n} \tag{9}$$

$$\tau_{ns} = \rho K \left[\frac{1}{1-N} \frac{\partial v}{\partial s} + \frac{u}{(1-n)\, R} + \frac{\partial u}{\partial n} \right] \tag{10}$$

where $K = CUh$ and $C = \frac{\kappa\sqrt{C_d}}{6} + \alpha_K$. The first term in the equation for C is a model for eddy viscosity and the α_K term is a correction factor (between 10^{-3} and 10^{-2}). Additionally, U is the free stream velocity. The bottom shear stress tensor terms are dealt with using the following drag coefficient closure as described in detail by *Nelson and McDonald* [1995].

$$(\tau_{zs}, \tau_{zn})_b = \rho C_d \sqrt{\langle u \rangle^2 + \langle v \rangle^2}\, \langle u, v \rangle \tag{11}$$

The drag coefficient (C_d) can be set by the user to a constant value over the entire model domain or calculated from a user specified roughness height (z_0) with the law of the wall (Equation 12).

$$C_d = \left[\frac{1}{\kappa} \left(\ln \frac{h}{z_0} - 1 \right) \right]^{-2} \tag{12}$$

For the uniform grain size sediment transport and conservation model utilized before mixed-grain-size capabilities were added by *Nelson et al.* [2015a], a single roughness height is specified for the entire domain. This allowed for some degree of spatially and temporally variable roughness based on flow depth; however, variable roughness due to surface grain-size spatial variability can not be accounted for. For the mixed-grain-size model developed by *Nelson et al.* [2015a], z_0 for each grid point is based on the grid point D_{84} particle size (particle size

for which 84% of the bed is finer) and a user specified empirical constant γ as follows:

$$z_0 = \gamma D_{84}. \tag{13}$$

γ has been found to be near 0.1 [*Hey*, 1979; *Whiting and Dietrich*, 1990; *Wiberg and Smith*, 1991; *Wilcock*, 1996]. This is a parameter that can be adjusted by the user to calibrate a model to measured conditions. This makes the roughness coefficient a function of both depth and grain size which allows the variable grain size on the bed to feedback on the flow field.

7.1.2 Sediment Transport

The sediment transport models available in the current version of FaSTMECH distributed with the iRIC interface assume uniform grain size and do not incorporate mixed-grain-size calculations. As part of the modifications made to FaSTMECH for the *Nelson et al.* [2015a] study, the *Parker* [1990] mixed-grain-size bedload equation was incorporated in the model. This bedload model has been shown to work well for gravel bedload transport conditions [*Lanzoni*, 2000; *Yager et al.*, 2007].

The *Parker* [1990] relation calculates a grain-size-specific dimensionless bedload transport rate, $W_i^\star$, defined as

$$W_i^\star = \frac{R_p g q_{bi}}{u_\star^3 F_i} \tag{14}$$

where R_p is the submerged specific gravity of sediment, q_{bi} is the volumetric bedload transport rate per unit width for the i^{th} grain-size class, $u_\star$ is the shear velocity, and F_i is the fraction of the i^{th} grain-size in the bed surface grain-size distribution. This parameter is used to calculate the bedload transport for the i^{th} grain-size class (q_{bi}). These grain-size specific bedload transport rates can be summed up to find the total bedload transport rate (q_{bT}). The ratio of each q_{bi} to q_{bT} can inform on the fraction of bedload transport within each i^{th} grain-size class. The dimensionless grain-size-specific bedload transport rate is calculated with empirical relationships based on the representative grain-size for each class, the geometric

mean grain-size, the geometric standard deviation of the grain-size, and Shields parameter ($\tau^\star = 0.0386$). Details of these relationships are presented by *Parker* [1990], as well as *Nelson et al.* [2015a].

Bedload transport equations such as the Parker formulation account for transport of sediment as a function of the boundary shear stress. In addition to this force, particles are also subject to gravitational forces. If the bed is not level (as is the case in rivers and flumes), this added force can alter the direction of movement away from the boundary shear stress vector. One way to account for this is to make an adjustment to the sediment transport vector, $\vec{q_{bi}}$. As channel bed slopes in alluvial channels are fairly shallow, particles are not subject to much gravitation force in the stream-wise direction. Additionally, if bedload transport in the cross-stream direction is minimal compared to stream-wise transport, the cross-stream transport, q_{in}, can be modified using the following equation derived by *Parker and Andrews* [1985]:

$$q_{in} = q_{is}\left[\frac{\tau_{bn}}{|\vec{\tau_b}|} - \Gamma\left(\frac{\tau^\star_{bi}}{\tau^\star_{ci}}\right)^{-n_t}\frac{\partial\eta}{\partial n}\right] \tag{15}$$

where the critical dimensionless shear stress, $\tau^\star_{ci}$, is calculated using a hiding relation defined by *Ashida and Michiue* [1972]. The value of Γ generally ranges between 1.5 and 5.4. Its effects were investigated by *Nelson et al.* [2015a], and a value of 1.2 was found to work best for the scenarios presented in that paper and this study.

7.1.3 Sediment Continuity with Stratigraphy

After the flow and sediment fields are calculated, bed evolution is calculated. This stage computes the change in elevation of the bed as well as the change in surface grain-size distribution. This is accomplished using the active layer method originally presented by *Hirano* [1971] and later modified for mixed-grain-size use by *Parker* [1992]. When integrating the stratigraphy framework, this active layer method is minimally changed to allow for access of the stored stratigraphy nodes described in Section 7.2.

Bed evolution due to transport of each grain size class is calculated from the Exner

equation of sediment transport [*Parker*, 1991]:

$$(1-\lambda_p)\left[f_{li}\frac{\partial}{\partial t}(\eta - L_a) + \frac{\partial F_i L_a}{\partial t}\right] = -\vec{\nabla}\cdot\vec{q_{bi}} \tag{16}$$

where q_{bi} is the grain size class specific volumetric bedload transport calculated previously, λ_p is the porosity (assumed equal to 0.35), f_{li} is the exchange fraction at the interface with the active layer, L_a is the active layer thickness ($L_a = 2D_{90}$), and F_i is the grain size fractions in the active layer (surface). Summing over all grain sizes, the change in bed elevation over time is

$$(1-\lambda_p)\frac{\partial \eta}{\partial t} = -\vec{\nabla}\cdot\vec{q_{bT}}. \tag{17}$$

The change in the surface grain-size distribution is then found by summing Equations 16 and 17:

$$(1-\lambda_p)\left[L_a\frac{\partial F_i}{\partial t} + (F_i - f_{li})\frac{\partial L_a}{\partial t}\right] = -\vec{\nabla}\cdot\vec{q_{bi}} + f_{li}\vec{\nabla}\cdot\vec{q_{bT}}. \tag{18}$$

Unlike the basic "three-layer model" utilized by *Nelson et al.* [2015a] where the subsurface grain size is homogeneous in time and space, the grain-size distribution associated with the subsurface layer can now vary with the stratigraphy framework. The details of how the subsurface grain size fractions are modified and stored during aggradation or degradation are presented in Section 7.2. Here I now look at how the surface interacts with the stored stratigraphy. This is accomplished through the exchange fraction term, f_{li}. If degradation is calculated according to Equation 17, then the exchange fraction is

$$f_{li} = f_i\big|_{z=\eta-L_a}. \tag{19}$$

That is, the exchange fraction takes on the grain size fractions stored in the stratigraphy node corresponding to the elevation of the bottom of the active layer. If aggradation occurs,

the exchange fraction is calculated as

$$f_{li} = \alpha \cdot F_i + (1 - \alpha)\, p_i, \tag{20}$$

where F_i and p_i are the surface and bedload grain size fraction of the i^{th} grain size respectively, and α is a user defined parameters defining the ratio of bedload to surface material mixed into the exchange fraction. The exchange fraction then is used to calculate the new surface grain-size distribution and well as the grain-size distribution stored in the stratigraphy nodes as later described in Section 7.2.

7.2 Stratigraphy Framework

As previously mentioned, the stratigraphy framework is a slightly modified version of the 1D morphodynamic model framework presented by *Viparelli et al.* [2010]. The primary modification is adding an additional spatial dimension to the framework as FaSTMECH is a 2D morphodynamic model. Some additional slight corrections were made to some of the equations presented by *Viparelli et al.* [2010], as well as a minor modification to allow use with large bed elevations (e.g. real world scenarios).

7.2.1 Initialization

The framework is initially set up as a 3D grid of stratigraphy nodes with the same stream wise and cross stream horizontal discretization as used for the surface domain, and a total of M_{max} evenly spaced nodes in the vertical. The spacing of the vertical nodes is the same as the stratigraphy layer thickness and is a user specified parameter (L_s). For preallocation purposes in Fortran a lower bounding elevation (B_l) and upper bounding elevation (B_u) are defined as

$$B_l = \text{FLOOR}\left(\eta_{min} - 0.1\eta_{min}\right) \tag{21}$$

and

$$B_u = \text{CEILING}\left(\eta_{max} + 0.1\eta_{max}\right) \tag{22}$$

where FLOOR is a function truncating to the lowest integer, CEILING is a function that rounds up to the highest integer value, η_{min} is the lowest bed elevation in the entire domain, and η_{max} is the maximum bed elevation in the entire domain. The total number of available (preallocated) nodes, M_{max}, is therefore

$$M_{max} = \text{FLOOR}\left(\frac{B_u - B_l}{L_s}\right) + 2. \tag{23}$$

While there are M_{max} stratigraphy nodes available at any single grid point, they will not be used since the bed elevation will remain below B_u (an error will occur if the bed evolves above this elevation). These inactive stratigraphy nodes can be thought of ghost nodes floating above the bed and contain no grain size information. The number of active stratigraphy nodes (which contain grain-size distribution information) is therefore the number of nodes that fit between the lower bounding elevation and the elevation at the bottom of the active layer. Note that most nodes have a spacing equal to L_s with the exception of the highest active stratigraphy node which has an elevation equal the elevation at the bottom of the active layer. Using the previously defined integer FLOOR function, the number of active stratigraphy nodes at location i, j is

$$M_{i,j} = \text{FLOOR}\left(\frac{\eta_{i,j} - L_{a\ i,j} - B_l}{L_s}\right) + 2 \tag{24}$$

where $\eta_{i,j}$ is the bed elevation, $L_{a\ i,j}$ is the active layer thickness, and the subscripts i and j are the stream wise and cross stream surface grid coordinates respectively. Note that this is one of the equations modified to allow for the use of large values for bed elevation.

Upon initialization of the stratigraphy grid, all active stratigraphy nodes are given the same initial bulk grain-size distribution as defined by the user. Furthermore, the elevation

of each stratigraphy node is stored. An example of the initial stratigraphy grid set up is shown for a single longitudinal slice (constant j coordinate) through the bed in Figure 23.

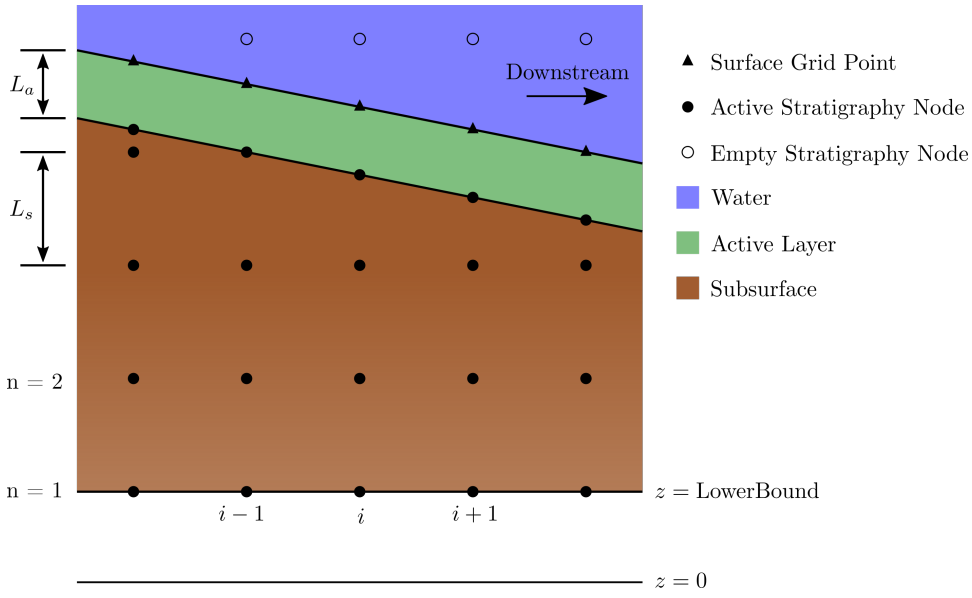

Figure 23: Longitudinal slice down arbitrary portion of model domain showing the initial stratigraphy grid set up.

7.2.2 Aggradation

There are three possible cases after the bed evolution is computed using the Exner equation: aggradation, the bed does not change, and degradation. This section will address the first case of aggradation of a specific grid point. A period of aggradation can be thought of as the "store" portion of the stratigraphy framework, in that grain size fractions from the exchange fraction calculated previously (mix of previous surface and bedload fractions) are saved in a subsurface stratigraphy node.

First, the number of active stratigraphy nodes for the new bed elevation and active layer thickness is computed using Equation 24. The framework is slightly different depending on whether the same number of stratigraphy nodes is needed or if additional stratigraphy nodes are needed. If no additional stratigraphy nodes are needed, then the grain size fractions stored in the top most stratigraphy node are computed as a thickness-weighted mix of the

exchange fraction and the existing fractions stored in the stratigraphy node:

$$f_{i,j,M,k}\ |_{t+\Delta t} = \frac{\left[f_{i,j,M,k}\left(\eta_{int\ i,j} - S_{i,j,M-1}\right)\right]_t + \delta_{i,j} f_{l\ i,j,k}}{\left[\eta_{int\ i,j} - S_{i,j,M-1}\right]_{t+\Delta t}} \tag{25}$$

where $f_{i,j,M,k}$ is the fraction of grain size class k in stratigraphy node M at grid point (i,j), $\eta_{int\ i,j}$ is the elevation of the interface between the active layer and subsurface at grid point (i,j), $S_{i,j,M-1}$ is the elevation of stratigraphy node $M-1$ at grid point (i,j), $\delta_{i,j}$ is the change in elevation of the interface between the bottom of the active layer and subsurface, and $f_{l\ i,j,k}$ is the fraction of grain size class k in the exchange fraction (Equation 20) at grid point (i,j). This a corrected and modified version of Equation 16 in *Viparelli et al.* [2010]. The value of $\eta_{int\ i,j}$ for time $t+\Delta t$ is then used to update the elevation of the top stratigraphy node ($S_{i,j,M}$). Stratigraphy node $M_{i,j}$ is the only node modified at (i,j) when the amount of aggradation is not enough to require the activation of another stratigraphy node.

If there is sufficient aggradation that additional stratigraphy nodes are needed as calculated by Equation 24, a slightly different frame is utilized for aggradation. The grain size fractions in the old top most stratigraphy node is computed as

$$f_{i,j,M-\Delta M,k}\ |_{t+\Delta t} = \frac{\left[f_{i,j,M,k}\left(\eta_{int\ i,j} - S_{i,j,M-1}\right)\right]_t}{L_s} + \frac{f_{l\ i,j,k}\left[S_{i,j,M-1} + L_s - \eta_{int\ i,j}\right]_t}{L_s} \tag{26}$$

where ΔM is the change in number of stratigraphy nodes from time t to $t+\Delta t$. Note that the stratigraphy node index for the terms on the right hand side refer to the conditions at the previous time step and not the new number of stratigraphy nodes at time $t+\Delta t$. The fractions in the stratigraphy node(s) above the old topmost node are simply equal to the exchange fraction (f_l) previously computed. The elevations of the new and previous top stratigraphy nodes are then adjusted accordingly with the new topmost stratigraphy node having an elevation equal to the elevation of the interface between the active layer and subsurface.

Figure 24 below depicts both of the above two scenarios. At $i-2$, the top most stratig-

raphy node is simply adjusted upward slightly. It would then take on a mix of its existing grain size fractions and the exchange fraction. As the amount of aggradation is relatively small in this location, the fractions stored in the top node would not change dramatically. At $i + 1$, a new stratigraphy node is activated. The old topmost node would have taken on a thickness weighted mixture of its antecedent grain size fractions and the fraction of the exchange fraction. As the bed aggraded more significantly at this locations, the change to the fractions for this node has the potential to be more substantial than the previous scenario (if the exchange fraction is considerably finer or coarser). The new stratigraphy node would simply take on the fractions in the exchange fractions.

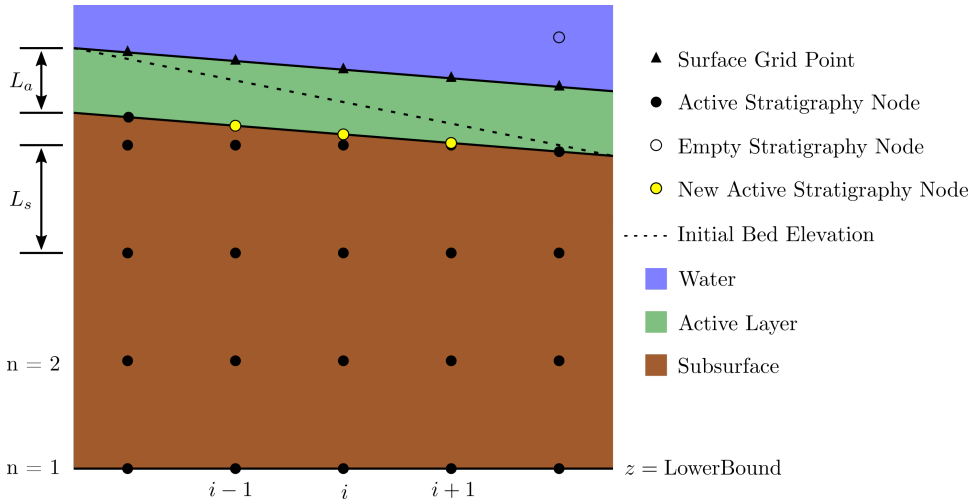

Figure 24: Stratigraphy grid modifications for a period of aggradation.

There is also the potential case of aggradation, but fewer stratigraphy nodes are needed. This would occur if the active layer thickness (a function of the 90th percentile grain size) is increased more than the amount of degradation. Therefore, while the bed surface may have aggraded, the elevation of the interface between the active layer and subsurface will have degraded. While this condition is unlikely, it is accounted for in the stratigraphy framework for robustness. If this occurs, the old top stratigraphy node is disabled and the node below it becomes the new topmost stratigraphy node. The elevation of this new top node is adjusted accordingly, but the grain size fractions stored in the node are not modified.

7.2.3 Degradation

As there would be no change to the stratigraphy grid if there is no local change in bed elevation, the other half of stratigraphy framework deals with the case of degradation. The degradation part of the stratigraphy routine is considerably more simple than the aggradation part; however, it is also the most important part of the framework. If the bed evolution routine cannot access the stored stratigraphy nodes then the stratigraphy cannot feed back on the flow and sediment transport fields.

In terms of accounting for changes in the stratigraphy grid, there are the same three cases as shown during aggradation: same number of stratigraphy nodes needed, fewer stratigraphy nodes needed, and more stratigraphy nodes needed. The first two fo these cases are shown in Figure 25. For all cases, the grain size fractions stored in the stratigraphy nodes are not

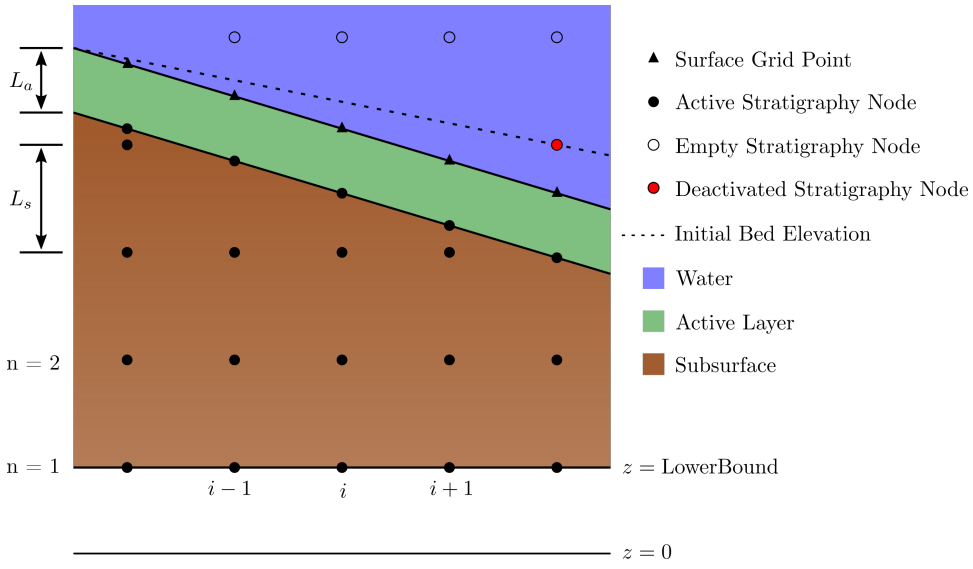

Figure 25: Modifications to the stratigraphy grid during degradation from the initial condition shown in Figure 23.

modified as material is assumed to only transfer out of the stratigraphy. Therefore, only node elevations need to be adjusted and/or nodes be deactivated. If the same number of stratigraphy nodes are needed as found with Equation 24, then only the elevation of the top most stratigraphy node is set equal to the active layer/subsurface interface elevation. If fewer nodes are needed according to Equation 24, then the nodes above the new topmost

stratigraphy node are deactivated and the elevation of the new top node adjusted to the interface elevation. In the unlikely case of more nodes needed, then a new stratigraphy node is activated and given grain size fractions equal to the old top most node's fractions. Then the elevations are adjusted accordingly.

Stratigraphy access during degradation is accomplished through the exchange fraction, f_l. During degradation, the exchange fraction is set equal to the fractions in the stratigraphy node to which the bed has degraded to. In the case of degradation through more than one stratigraphy node, the fractions are set equal to the fractions in the lowest of the stratigraphy nodes degraded through. This negates the potential effects of degrading through the higher stratigraphy nodes which may have quite different grain-size distributions. With the short time steps used here, degradation through multiple layers is unlikely.